



1 **Sea salt reactivity over the northwest Atlantic: An in-depth look**
2 **using the airborne ACTIVATE dataset**

3
4 Eva-Lou Edwards¹, Yonghoon Choi^{2,3}, Ewan C. Crosbie^{2,3}, Joshua P. DiGangi², Glenn S.
5 Diskin², Claire E. Robinson^{2,3,†}, Michael A. Shook², Edward L. Winstead^{2,3}, Luke D. Ziemba²,
6 and Armin Sorooshian^{1,4}

7
8
9 ¹Department of Chemical and Environmental Engineering, University of Arizona, Tucson, AZ,
10 85721, USA

11 ²NASA Langley Research Center, Hampton, VA, 23681, USA

12 ³Analytical Mechanics Associates, Inc., Hampton, VA, 23666, USA

13 ⁴Department of Hydrology and Atmospheric Sciences, University of Arizona, Tucson, AZ,
14 85721, USA

15
16 [†]Deceased

17
18 *Corresponding author: armin@arizona.edu



19 Abstract

20 Chloride (Cl^-) displacement from sea salt particles is an extensively studied phenomenon with
21 implications on human health, visibility, and the global radiation budget. Past works have
22 investigated Cl^- depletion over the northwest Atlantic (NWA), yet an updated, multiseasonal, and
23 geographically expanded account of sea salt reactivity over the region is needed. This study uses
24 chemically resolved mass concentrations and meteorological data from the airborne Aerosol Cloud
25 meTeorology Interactions oVer the western ATlantic Experiment (ACTIVATE) to quantify
26 seasonal, spatial, and meteorological trends in Cl^- depletion and to explore the importance of
27 quantifying (1) non-sea salt sources of Na^+ and (2) mass concentrations of lost Cl^- instead of
28 relative amounts displaced. Lost Cl^- mass concentrations are lowest in December-February and
29 March, moderate around Bermuda in June, and highest in May (median losses of 0.04, 0.04, 0.66,
30 and $1.76 \mu\text{g m}^{-3}$, respectively), with losses in May high enough to potentially accelerate
31 tropospheric oxidation rates. Inorganic acidic species can account for all Cl^- depletion in
32 December-February, March, and June near Bermuda, yet none of the lost Cl^- in May, suggesting
33 organic acids may be of importance for Cl^- displacement in certain months. Contributions of dust
34 to Na^+ are not important seasonally but may cause relevant overestimates of lost Cl^- in smoke and
35 dust plumes. Higher percentages of Cl^- depletion often do not correspond to larger mass
36 concentrations of lost Cl^- , so it is highly recommended to quantify the latter to place depletion
37 reactions in context with their role in atmospheric oxidation and radiative forcing.

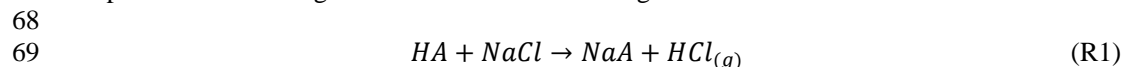


38 1. Introduction

39 Chlorine (Cl) is a common constituent of trace gases and aerosol particles found in Earth's
40 atmosphere. Chlorine-containing species play a critical role in the global radiation budget for many
41 reasons, including their ability to produce highly reactive Cl radicals. These radicals can perturb
42 atmospheric chemical processes by inducing reactions that would otherwise be less likely to occur
43 and/or accelerating the rates of certain reactions. For example, Cl radicals in the stratosphere can
44 incite reactions that destroy ozone (O₃; Molina and Rowland, 1974; Solomon et al., 2023),
45 therefore allowing increased amounts of shortwave radiation to reach the surface and harmfully
46 affect living beings.

47 Cl radicals typically react faster with volatile organic compounds (VOCs) compared to
48 hydroxyl radicals (OH; Roberts et al., 2008; Thornton et al., 2010; Young et al., 2014), which has
49 particular importance in the troposphere. Cl radicals oxidize methane ~16 times faster than OH
50 (Faxon and Allen, 2013 and references therein), thus reducing the lifetime of this important
51 greenhouse gas. Accelerated oxidation of methane and other VOCs can result in increased O₃
52 production near the surface (Knipping and Dabdub, 2003; Pechtl and von Glasow, 2007; Tanaka
53 et al., 2003), which can have deleterious effects on animals (e.g., respiratory problems, increased
54 mortality; Lippmann, 1989; Nuvolone et al., 2018) and plants (e.g., decreased growth and
55 photosynthesis; Wittig et al., 2009). Cl radicals may be responsible for 15 – 27% of VOC oxidation
56 in the global troposphere (Sherwen et al., 2016) and can play an exceptionally critical role in
57 governing atmospheric composition in the early morning when OH radicals are less abundant
58 (Young et al., 2013; Riedel et al., 2014; Osthoff et al., 2008). Due to their significant impacts on
59 radiative forcing, rates of chemical cycling, and the health of living organisms, it is critical to
60 quantify and understand sources of atmospheric Cl radicals.

61 Sea salt aerosol particles are the largest reservoir of reactive atmospheric Cl. Keene et al.
62 (1999) estimates that at any given time there are ~22 Tg of reactive Cl in the troposphere, and that
63 68% of this mass is found in particulate form, primarily sea salt. Although the Cl in sea salt will
64 not directly photolyze to produce Cl radicals, it can be displaced by acidic species (e.g., sulfate
65 [SO₄²⁻], nitrate [NO₃⁻], organic acids) and released in a reactive gaseous form (e.g., ClNO₂, HCl,
66 Cl₂) that has the potential to produce Cl radicals. This phenomenon is called chloride (Cl⁻)
67 depletion and can be generalized with the following reaction:



71 where A is one of the acidic species mentioned above. In addition to producing reactive chlorine-
72 containing gases, Cl⁻ depletion can alter the acidity (e.g., Keene and Savoie, 1998), hygroscopicity
73 (e.g., Drozd et al., 2014; Ghorai et al., 2014; Randles et al., 2004), and optical properties
74 (Finlayson-Pitts and Pitts, 2000; Tang et al., 1997) of sea salt particles. Such changes affect
75 partitioning of other chemicals (e.g., water vapor, ammonia [NH₃⁺], SO₄²⁻, NO₃⁻) between the gas
76 and particle phases (Chen et al., 2021), the rates and types of reactions occurring within sea salt
77 particles (Chameides and Stelson, 1993), the activity of these particles as cloud condensation
78 nuclei (e.g., Chatterjee et al., 2020), and their interactions with solar radiation, all of which can
79 have implications for visibility, air quality, biogeochemical cycles, and Earth's radiation budget.

80 Many factors dictate the extent to which Cl⁻ depletion occurs in an air mass including
81 meteorology (e.g., wind speed, temperature, relative humidity [RH], available solar radiation), the
82 size distribution and mixing state of sea salt particles, and the availability and length of exposure
83 to surrounding acidic species (Su et al., 2022 and references therein). Regarding the latter, Cl⁻



84 depletion is therefore typically observed where marine particles and acidic species are both
85 present, such as where emissions from biomass burning (BB) advect over a marine location (Braun
86 et al., 2017; Maudlin et al., 2015; Li et al., 2003; Yokelson et al., 2009; Akagi et al., 2013; Dang
87 et al., 2022; Crosbie et al., 2022), in regions with active phytoplankton and marine bacteria that
88 emit dimethyl sulfide (DMS), which can oxidize to form sulfuric acid (H_2SO_4 ; Seinfeld and Pandis,
89 2016; Tang et al., 2019; Yan et al., 2020), and/or in and around urban coastal environments (e.g.,
90 Kong et al., 2014; Chatterjee et al., 2020; AzadiAghdam et al., 2019; Nolte et al., 2008) where
91 anthropogenic emissions serve as precursors for various acidic species.

92 For this reason, the northwest Atlantic (NWA) is an opportune region for observing and
93 studying Cl^- depletion. Cities extending along the East Coast of North America consistently emit
94 sulfur dioxide (SO_2), nitrogen oxides (NO_x), and VOCs, which can oxidize to form H_2SO_4 , nitric
95 acid (HNO_3), and organic acids, respectively, while sea salt particles are ubiquitous over the region
96 due to wave breaking (Reid et al., 2001; Ferrare et al., 2023). Occasional long-range transport from
97 BB in Alaska, Canada, and the western United States (U.S.; Fehsenfeld et al., 2006; Mardi et al.,
98 2021), agricultural fires throughout the eastern and southeastern U.S. (Jaffe et al., 2020; McCarty
99 et al., 2007), wintertime wood burning for residential heating (Corral et al., 2021; Sullivan et al.,
100 2019), and seasonally varying emissions from vegetation and ocean biological activity (Savoie et
101 al., 2002; Corral et al., 2022) can also introduce acidic species to this region.

102 Cl^- depletion has been observed over the NWA for decades (Table 1). Previous datasets
103 typically span 2 – 3 months, and most are reflective of conditions during the boreal summer,
104 although there are a handful of studies extending outside of this period (i.e., Keene et al., 1990;
105 Yao and Zhang, 2012; Zhao and Gao, 2008; Haskins et al., 2018). Combining results from these
106 works to build seasonal and temporal statistics is challenged by the fact that each dataset is specific
107 to a certain altitude (or range of altitudes), location(s), time period, sampling method, and size
108 range of sampled particles. In addition to these logistical constraints, there is an overall shortage
109 of Cl^- depletion data for the spring, fall and winter, which is of concern as depletion processes are
110 sensitive to several properties that fluctuate seasonally over the NWA (e.g., temperature, solar
111 radiation, RH).

112 Most past works over the NWA report on Cl^- depletion along the United States East Coast
113 (USEC) and/or at Bermuda. To our knowledge, there is an absence of discussion about the gradient
114 in Cl^- depletion moving from the USEC to the open ocean environment closer to Bermuda. Corral
115 et al. (2021) showed strong gradients in aerosol optical depth along this direction for several
116 particle types including sea salt and SO_4^{2-} , suggesting there may be a gradient in Cl^- depletion as
117 well. Furthermore, Cl^- depletion results from previous studies typically reflect conditions near the
118 surface, yet Shinozuka et al. (2004) showed that the vertical scattering profile of sea salt in the
119 lower 1 km of the atmosphere becomes increasingly less uniform with increasing wind speed. Also
120 of note is that most datasets referenced in Table 1 are now several decades old. Mass
121 concentrations of SO_2 , NO_x , SO_4^{2-} , and NO_3^- over the eastern U.S. and Canada have steadily
122 decreased since 1990 due, in part, to the Clean Air Act of 1963 and its subsequent amendments
123 (Feng et al., 2020; Kuklinska et al., 2015). Such reductions warrant an updated analysis of Cl^-
124 depletion over the NWA.

125 We note that Cl^- depletion results from the Wintertime Investigation of Transport, Emissions
126 and Reactivity (WINTER) aircraft campaign (Haskins et al., 2018) are an exception to many of
127 the points raised above. As an airborne campaign from February – March 2015, WINTER provides
128 data relevant to halogen chemistry at altitudes throughout the boundary layer, at a time of year that
129 had previously not been studied, and in a year recent enough to capture the aforementioned



130 reductions in anthropogenically sourced acidic species. However, WINTER flights specifically
131 sampled over and downwind of various pollution sources in the eastern and southeastern U.S.,
132 meaning Cl^- depletion results may be disproportionately reflective of highly polluted, coastally
133 influenced air masses as compared to other air mass types observed over the NWA during winter
134 and spring (e.g., those (i) occurring after synoptically forced frontal systems have moved through,
135 (ii) associated with cold air outbreaks (CAOs), and (iii) occurring when southerly winds advect
136 maritime air masses northward along the East Coast).

137 It is common for Cl^- depletion studies to base their calculations on the assumption that sea salt
138 particles are the only source of atmospheric sodium (Na^+ ; i.e., Na^+ is used as the reference species
139 for determining the extent of Cl^- depletion observed), including nearly all the works listed in Table
140 1. The validity of this assumption is dependent on several factors, including the proximity to urban
141 emissions, if dust particles are present, and the size range of particles sampled. Ooki et al. (2002)
142 found Na^+ to be highly correlated with potassium (K^+) in particles $< 1.1 \mu\text{m}$ in urban air masses,
143 implying that these two species have the same source in fine, anthropogenically sourced particles.
144 K^+ is thought to come mainly from BB (Echalar et al., 1995; Andreae et al., 1998; Andreae and
145 Merlet, 2001) and anthropogenic activities (Ooki et al., 2002 and references therein), suggesting
146 that marine air masses heavily influenced by BB or urban emissions may have nonnegligible
147 contributions from non-sea salt sources to total Na^+ , especially if submicron particles contribute
148 significantly to total mass concentrations (which would depend on the size range of particles
149 sampled). Na^+ can also be found in mineral dust (Seinfeld and Pandis, 2016), which has motivated
150 a handful of studies to discern between the amounts of Na^+ coming from dust and sea salt using a
151 system of equations (e.g., Boreddy and Kawamura, 2015; AzadiAghdam et al., 2019). The NWA
152 is known to be periodically influenced by Asian, African, and North American dust (e.g., Aldhaif
153 et al., 2020) and emissions from BB (Fehsenfeld et al., 2006; Schroder et al., 2018; Sullivan et al.,
154 2019; Mardi et al., 2021), and is consistently influenced by anthropogenic activities throughout
155 the year. Several works shown in Table 1 have acknowledged that these additional sources of Na^+
156 may influence estimates of Cl^- depletion over the NWA, but none have quantitatively explored this
157 possibility.

158 Finally, most Cl^- depletion studies report the percentage of Cl^- in unreacted sea salt particles
159 that has been displaced by acidic species, an approach useful for quantifying the extent of Cl^-
160 depletion processes independently of the sea salt mass concentrations present, which can vary
161 seasonally, temporally, and geographically. However, reporting Cl^- depletion as a percentage can
162 make it more difficult to conceptualize and quantify the degree to which depletion reactions may
163 be affecting atmospheric oxidation potential. Several past works focusing on the NWA have
164 reported the magnitude of Cl^- displaced from sea salt particles, either in units of nmol m^{-3} (e.g.,
165 Keene and Savoie, 1998; Keene et al., 1990) or pptv (Keene et al., 2007; Haskins et al., 2018),
166 which we find useful for comprehensive interpretation considering that Singh and Kasting (1988)
167 suggested ppbv concentrations of gaseous and reactive Cl species (e.g., HCl) have the potential to
168 produce enough Cl radicals to oxidize 20 – 40% of nonmethane alkanes in the marine troposphere.
169 Thus, reporting Cl^- depletion both as a percentage and as a mass concentration benefits the
170 atmospheric chemistry community as results can be used either comparatively or to improve
171 quantification of Cl radical budgets and the atmospheric oxidation capacity in a given region.
172 Although a few past works in the NWA have reported mass concentrations of displaced Cl^- , there
173 is still a need for results reflecting current conditions across a range of seasons as we have
174 discussed above.



175 In summary, there is a demand for an updated, multi-seasonal, spatially resolved dataset
176 reflecting Cl⁻ depletion processes in the NWA boundary layer across a variety of meteorological
177 conditions and air mass types. There is also interest in (i) exploring the sensitivity of Cl⁻ depletion
178 results to accounting for non-sea salt sources of Na⁺, especially in seasons and/or air masses
179 influenced by dust and BB emissions, as well as (ii) quantifying both the percentage and magnitude
180 of Cl⁻ displaced from sea salt particles for straightforward comparisons to other works and to link
181 results more easily to boundary layer Cl radical budgets and their potential influence on
182 atmospheric oxidation rates. This study seeks to address these points by using data from the NASA
183 Aerosol Cloud meTeorology Interactions oVer the western ATlantic Experiment (ACTIVATE)
184 airborne field campaign (Sorooshian et al., 2019). The statistical approach, large number of flights
185 spanning a range of seasons and meteorological conditions, and type of instruments deployed on
186 this campaign make the ACTIVATE dataset well-suited to address several of the outstanding
187 uncertainties and unknowns regarding Cl⁻ depletion over the NWA.



188 **Table 1.** Relevant information from previous works, sorted chronologically, documenting Cl⁻
 189 depletion over the Northwest Atlantic (NWA). “USEC” stands for United States East Coast, and
 190 “U.S.” stands for United States.

Reference(s)	Dates	Location	Platform(s)	Reference species to determine Cl ⁻ depletion	Discusses possibility of non-sea salt sources of Na ⁺ and/or Cl ⁻
Keene et al. (1990)	Jul – Sep 1988	USEC and near Bermuda	Ship and aircraft	Na ⁺	No
Keene and Savoie (1998)	Apr – May 1996	Bermuda	Surface station	Na ⁺	No
Nolte et al. (2008)	May – Jun 2002	Tampa, Florida (U.S.)	Surface stations	Na ⁺	Yes
Yao and Zhang (2012)	Jun – Jul 2002, Oct – Nov 2002	Kejimikujik, Nova Scotia	Surface station	Na ⁺	No
Keene et al. (2004)	Jul – Aug 2002	USEC	Ship	Mg ²⁺ . ²	No
Quinn and Bates (2005)	Jul – Aug 2002	USEC	Ship	Na ⁺	No
Keene et al. (2007)	Jul – Aug 2004	Appledore Island, Maine (U.S.)	Surface station	Na ⁺ and Mg ²⁺	Yes
Zhao and Gao (2008)	Jul – Sep 2006	Newark, New Jersey (U.S.)	Surface station	Na ⁺	Yes
Bondy et al. (2017)	Jun – Jul 2011	Centreville, Alabama (U.S.)	Surface station	Na ⁺ and Mg ²⁺	Yes
Haskins et al. (2018)	Feb – Mar 2015	USEC and over land around major pollution sources across the eastern U.S. ¹	Aircraft	Na ⁺	Yes

191 ¹The Wintertime Investigation of Transport, Emissions, and Reactivity (WINTER) airborne field
 192 campaign focused on three regions over the U.S.: i) the northeast metropolitan corridor
 193 (encompassing major cities from Boston to Washington D.C.), ii) the Ohio River Valley, and iii)
 194 the Southeast. Research flights also extended over coastal waters to sample polluted air masses
 195 downwind from their sources.

196 ²Magnesium (Mg²⁺) was chosen as the reference species for sea salt in Keene et al. (2004) as Na⁺
 197 had a relatively higher and more variable background in the quartz-fiber sampling media used.



198

199 **2. Data and methods**

200 **2.1 ACTIVATE campaign description**

201 The ACTIVATE field campaign focused on characterizing relationships between aerosol
202 particles, meteorology, and marine boundary layer clouds over the NWA using two research
203 aircraft flying in coordination. Operations were based out of NASA Langley Research Center
204 (LaRC), although a multitude of other sites supported various aspects of the project. The high-
205 flying King Air usually flew steadily at ~9 km releasing dropsondes and using a suite of remote
206 sensors to retrieve particle and cloud properties below the aircraft. The low-flying HU-25 Falcon
207 (hereafter referred to as the “Falcon”) made in situ measurements of trace gases, aerosol particle
208 properties, cloud and precipitation properties (if present), and meteorological conditions in and
209 around boundary layer clouds or in clear conditions usually below 3 km.

210 ACTIVATE placed a high priority on building statistics to fulfill its objectives and address
211 current uncertainties regarding aerosol-cloud interactions and remote sensing capabilities over the
212 NWA. To acquire such statistics, the Falcon and King Air achieved 174 and 168 flights with 574
213 and 592 total flight hours, respectively, from 2020 – 2022 (note that 162 of these were “joint”
214 flights where the aircraft flew in coordination; Sorooshian et al., 2023). The campaign included
215 multiple seasons, with each aircraft adhering to an intentional and consistent flight strategy
216 throughout, to better constrain the multitude of variables affecting a given clear or cloudy scene.
217 As mentioned above, the King Air flew fixedly at ~9 km regardless of the amount of cloud
218 coverage below. In the presence of low-level (<3 km) clouds, the Falcon conducted “cloud
219 ensembles” by flying 3-minute legs at the following key vertical positions: near the ocean surface
220 (MinAlt; ~150 m), below cloud base, above cloud base, below cloud top, and above cloud top. In
221 the absence of low-level clouds, the Falcon switched to “clear ensembles,” which involved 3-
222 minute legs at MinAlt, ~230 m (an altitude useful for remote sensing validation), and at altitudes
223 falling slightly below and above the boundary layer height (see Fig. 2 in Sorooshian et al. [2023]
224 for an illustration of these ensembles). The campaign was executed over six deployments, which
225 are referred to as Winter 2020 (February – March 2020), Summer 2020 (August – September
226 2020), Winter 2021 (January – April 2021), Summer 2021 (May – June 2021), Winter 2022
227 (November 2021 – March 2022), and Summer 2022 (May – June 2022) as recommended in
228 Sorooshian et al. (2023). Note that Winter 2022 includes two months in 2021 but is referred to as
229 “Winter 2022” for simplicity.

230

231 **2.2 Falcon data**

232 The main instrument providing data for this study is a particle into liquid sampler (PILS;
233 Brechtel Manufacturing Inc. [BMI]) that was operated downstream from an isokinetic Clarke-style
234 shrouded solid double-diffuser inlet (BMI; McNaughton et al., 2007) onboard the Falcon. The
235 PILS grows aerosol particles with diameters of 50 - 5000 nm at ambient RH into droplets large
236 enough to be collected via inertial impaction (Sorooshian et al., 2006; Crosbie et al., 2020).
237 Droplets striking the impaction plate are pumped into vials that are analyzed offline using ion
238 chromatography (IC) to quantify air equivalent mass concentrations of Na⁺, ammonium (NH₄⁺),
239 K⁺, magnesium (Mg²⁺), calcium (Ca²⁺), Cl⁻, NO₃⁻, SO₄²⁻, and oxalate. PILS data are critical to this
240 study due to the instrument’s ability to capture particles containing sea salt, dust, and other
241 refractory species that are largely omitted by the aerosol mass spectrometer (AMS). PILS flowrates
242 were set such that it took 300 - 420 s (5 – 7 minutes) to fill each vial, the minimum duration for
243 collecting enough particle mass to be above speciated detection limits while also meeting injection



244 volume requirements for IC analysis. Note that the time spent collecting one PILS sample is greater
245 than the duration of the individual level legs (~3 minutes) comprising clear and cloudy ensembles.
246 The possibility that each PILS sample could represent atmospheric properties sampled during
247 multiple level legs and/or periods of ascent or descent between level legs impacted our analysis in
248 two ways. First, PILS measurements must be considered as a representation of water-soluble ionic
249 composition throughout the lower 3 km of the atmosphere, meaning they cannot provide vertically
250 resolved information. Second, we exclude PILS data collected during cloudy ensembles to
251 eliminate possible cloud contamination. During cloudy ensembles, it is likely that the Falcon
252 intercepted a cloud within any interval of 5 – 7 minutes, and in doing so, shattered droplets and
253 other cloud artifacts were collected in the awaiting sample vial. Additionally, while flying through
254 clouds, large droplets and ice particles can impact onto the walls within the isokinetic inlet where
255 they may resuspend and, therefore, cause delayed sampling, of larger particles previously caught
256 on these walls.

257 The PILS was operated without upstream acid and base denuders, which opened the possibility
258 for soluble gases (e.g., NH_3) to contribute to speciated mass concentrations. During quality control
259 analyses, PILS NH_4^+ mass concentrations were unjustifiably high in many samples, prompting us
260 to omit this species from this study's analysis. As NH_4^+ is a critical species for deriving parameters
261 relevant to Cl^- depletion, we alternatively use NH_4^+ mass concentrations from a high-resolution
262 time-of-flight aerosol mass spectrometer (HR-ToF-AMS; Aerodyne; DeCarlo et al., 2008;
263 hereafter referred to as an "AMS"), which provided non-refractory mass concentrations of NH_4^+
264 (among other species) for particles 60 – 600 nm in diameter at a 30-s time resolution. The AMS
265 additionally provided mass concentrations of spectral markers for organic components, of which
266 we use the tracers for oxygenated organics, m/z 44, and methanesulfonic acid (MSA), m/z 79. AMS
267 data were filtered to isolate those from clear ensembles and then averaged over the 5- to 7-minute
268 interval for each PILS sample. Due to differences in the size range of the PILS and AMS, NH_4^+
269 mass concentrations from the AMS represent a lower limit in this analysis.

270 Horizontal wind speed and static air temperature data were obtained using the Turbulent Air
271 Motion Measurement System (TAMMS; Thornhill et al., 2003) operating at 20 Hz time resolution,
272 while the diode laser hygrometer (DLH; Diskin et al., 2002) supplied water vapor mixing ratios
273 and values of RH at 1 Hz time resolution. A commercial cavity ringdown spectrometer (G2401-
274 m; PICARRO, Inc.) provided carbon monoxide (CO) measurements at 0.4 Hz resolution (DiGangi
275 et al., 2021), which are used to qualitatively compare the extent to which certain seasons were
276 influenced by anthropogenic emissions (Panagi et al., 2020; Naeher et al., 2001; Saide et al., 2011).
277 Data are only considered from clear ensembles for each of the parameters described in this
278 paragraph.

279 The Falcon occasionally intercepted clouds during clear ensembles. During these cloud passes,
280 certain instruments (e.g., the AMS) sampled downstream of a counterflow virtual impactor (CVI;
281 BMI; Shingler et al., 2012) for droplet residual characterization. We removed data collected during
282 periods with active CVI sampling from our analysis for all variables mentioned above.

284 **2.3 Deployment selection and season/category classifications**

285 This analysis focuses on data collected during the Winter 2022 and Summer 2022
286 deployments as they cover the largest geographical range over the NWA, thus presenting the best
287 opportunity for studying spatial gradients in Cl^- depletion. During Winter 2022, sampling was
288 extended northward on flights when the Falcon flew to Quonset State Airport in Rhode Island,
289 refueled, and returned to LaRC, an option that was unavailable during the first four deployments



290 due to challenges associated with the COVID-19 pandemic. Summer 2022 is the only deployment
291 to (i) execute “transit flights” (i.e., flights where the Falcon flew to Bermuda, refueled, and flew
292 back to LaRC on the same day) and (ii) include a set of out-and-back flights based in Bermuda.
293 Additionally, Winter 2022 and Summer 2022 supply the largest and most continuous dataset
294 compared to the first two years of the campaign. Nearly half of the total Falcon flights occurred
295 within these two deployments, and sampling occurred consistently from 31 November 2021 to 18
296 June 2022 with a brief break from 30 March – 02 May 2022. The high frequency of flights over a
297 ~7-month period allows us to explore the seasonal evolution of properties relevant to Cl⁻ depletion,
298 while also observing their fluctuations on daily to multiday time scales.

299 To capture both seasonal and spatial trends, Winter 2022 and Summer 2022 data are distributed
300 among the following categories by season/month and/or by the geographical area sampled:
301 December-February (30 November 2021 – 26 February 2022), March (02 – 29 March 2022), May
302 (03 – 20 May 2022), March transit (22 March 2022), May transit (18, 21, and 31 May 2022), and
303 June Bermuda (02 – 13 June 2022). Note that some flights from the Winter 2022 and Summer
304 2022 deployments are omitted from this study because they are either composed entirely of cloudy
305 ensembles and/or PILS data are unavailable during the clear ensembles. To explore relationships
306 between (i) speciated mass concentrations and Cl⁻ depletion, and (ii) phenomena occurring on finer
307 time scales (e.g., the passage of weather fronts, transport events of African dust plumes),
308 meteorological conditions and/or notable influence from distinct aerosol types are documented for
309 each research flight (RF). We also select RFs sampling various airstreams associated with passing
310 frontal systems and dust-influenced air masses to further illustrate relationships between these
311 phenomenon and properties relevant to Cl⁻ depletion.

312

313 **2.4 Calculations relevant to Cl⁻ depletion**

314 The following section describes how various properties associated with Cl⁻ depletion were
315 derived using PILS and AMS bulk speciated mass concentrations and literature-based ratios for
316 ions in sea salt, dust, and emissions from various combustion processes. Identifying the amount of
317 Cl⁻ displaced from sea salt particle begins with quantifying the original amount of Cl⁻, which we
318 derive from Na⁺ in sea salt (ssNa⁺) as this species has a relatively high mass fraction and is
319 chemically inert in sea salt particles. We use Eqs. 1 – 5 to resolve contributions of sea salt and dust
320 to bulk PILS mass concentrations of Na⁺ and Ca²⁺ (see Sect. S1 in the Supplement for additional
321 information about these equations, Table S1 for variable nomenclature, and Table S2 for values of
322 constant parameters [e.g., mass ratios]).

323

$$Na_{bulk}^{+} = ssNa^{+} + Na_{dust}^{+} \quad 1$$

$$Ca_{bulk}^{2+} = ssCa^{2+} + Ca_{dust}^{2+} \quad 2$$

$$ssCa^{2+} = ssNa^{+} \cdot \left(\frac{Ca^{2+}}{Na^{+}} \right)_{ss} \quad 3$$

$$Ca_{dust}^{2+} = Na_{dust}^{+} \cdot \left(\frac{Ca^{2+}}{Na^{+}} \right)_{dust} \quad 4$$



$$ssNa^+ = \frac{Ca_{bulk}^{2+} - Na_{bulk}^+ \cdot \left(\frac{Ca^{2+}}{Na^+}\right)_{dust}}{\left(\frac{Ca^{2+}}{Na^+}\right)_{ss} - \left(\frac{Ca^{2+}}{Na^+}\right)_{dust}} \quad 5$$

324 We then use an analogous set of equations (Eqs. 6 – 14) to explore if various combustion
 325 processes contribute nonnegligible amounts of Na^+ to bulk PILS Na^+ mass concentrations (see
 326 Sect. S2 for more information).

$$Na_{bulk}^+ = ssNa^+ + Na_{dust}^+ + Na_{comb}^+ \quad 6$$

$$Ca_{bulk}^{2+} = ssCa^{2+} + Ca_{dust}^{2+} \quad 7$$

$$K_{bulk}^+ = ssK^+ + K_{dust}^+ + K_{comb}^+ \quad 8$$

$$ssCa^{2+} = ssNa^+ \cdot \left(\frac{Ca^{2+}}{Na^+}\right)_{ss} \quad 9$$

$$Ca_{dust}^{2+} = Na_{dust}^+ \cdot \left(\frac{Ca^{2+}}{Na^+}\right)_{dust} \quad 10$$

$$ssK^+ = ssNa^+ \cdot \left(\frac{K^+}{Na^+}\right)_{ss} \quad 11$$

$$K_{dust}^+ = Ca_{dust}^{2+} \cdot \left(\frac{K^+}{Ca^{2+}}\right)_{dust} \quad 12$$

$$Na_{comb}^+ = K_{comb}^+ \cdot \left(\frac{Na^+}{K^+}\right)_{comb} \quad 13$$

$$ssNa^+ = \frac{Na_{bulk}^+ - K_{bulk}^+ \cdot \left(\frac{Na^+}{K^+}\right)_{comb} + Ca_{bulk}^{2+} \cdot \left[\left(\frac{K^+}{Ca^{2+}}\right)_{dust} \cdot \left(\frac{Na^+}{K^+}\right)_{comb} - \left(\frac{Na^+}{Ca^{2+}}\right)_{dust}\right]}{1 - \left[\left(\frac{Ca^{2+}}{Na^+}\right)_{ss} \cdot \left(\frac{K^+}{Ca^{2+}}\right)_{dust} \cdot \left(\frac{Na^+}{K^+}\right)_{comb}\right] - \left[\left(\frac{K^+}{Na^+}\right)_{ss} \cdot \left(\frac{Na^+}{K^+}\right)_{comb}\right] - \left[\left(\frac{Ca^{2+}}{Na^+}\right)_{ss} \cdot \left(\frac{Na^+}{Ca^{2+}}\right)_{dust}\right]} \quad 14$$

327

328 Combustion-generated particles over the NWA can stem from a range of seasonal and
 329 perennial processes, each with a different Na^+ and K^+ emission factor. We use empirical, literature-
 330 based values of $\left(\frac{Na^+}{K^+}\right)_{comb}$ for particles emitted from the following combustion-related
 331 activities/phenomena: agricultural burning, forest fires, industrial operations, sauna stove wood
 332 burning for residential heating, car driving, and coal burning for electricity generation (Table S3).
 333 Note that only one value at a time can be used for $\left(\frac{Na^+}{K^+}\right)_{comb}$ in Eqs. 13 and 14, which forces the
 334 assumption that all combustion-generated particles collected in PILS samples are from the same
 335 source and/or have the same $\left(\frac{Na^+}{K^+}\right)_{comb}$ value.

336 Mass concentrations of $ssNa^+$ determined either by Eqs. 1 – 5 or Eqs. 6 – 14 are then used to
 337 determine sea salt mass concentrations (Eq. 15) as well as quantities relevant to Cl^- depletion (Eqs.
 338 16 – 26).



$$Sea\ salt = ssNa^+ \cdot \left(\frac{total\ mass}{Na^+} \right)_{ss} \quad 15$$

$$\%Cl^- \text{ depletion} = 100 \cdot \frac{ssNa^+ \cdot \left(\frac{Cl^-}{Na^+} \right)_{ss} - Cl_{bulk}^-}{ssNa^+ \cdot \left(\frac{Cl^-}{Na^+} \right)_{ss}} \quad 16$$

$$Lost\ Cl^- = ssNa^+ \cdot \left(\frac{Cl^-}{Na^+} \right)_{ss} - Cl_{bulk}^- \quad 17$$

$$Lost\ Cl_{bulk}^- = Na_{bulk}^+ \cdot \left(\frac{Cl^-}{Na^+} \right)_{ss} - Cl_{bulk}^- \quad 18$$

$$Lost\ Cl_{diff}^- = Lost\ Cl_{bulk}^- - Lost\ Cl^- \quad 19$$

$$nssSO_4^{2-} = SO_{4,bulk}^{2-} - ssNa^+ \cdot \left(\frac{SO_4^{2-}}{Na^+} \right)_{ss} \quad 20$$

$$ExSO_4^{2-} = nssSO_4^{2-} - \frac{MW_{SO_4^{2-}}}{MW_{NH_4^+}} \cdot \frac{NH_{4,bulk}^+}{y_{SO_4^{2-}}} \quad 21$$

$$ExNH_4^+ = NH_{4,bulk}^+ - \frac{MW_{NH_4^+}}{MW_{SO_4^{2-}}} \cdot y_{SO_4^{2-}} \cdot nssSO_4^{2-} \quad 22$$

$$ExNO_3^- = NO_{3,bulk}^- - \frac{MW_{NO_3^-}}{MW_{NH_4^+}} \cdot \frac{ExNH_4^+}{y_{NO_3^-}} \quad 23$$

$$Excess\ acidic\ species = ExSO_4^{2-} + ExNO_3^- + oxalate_{bulk} \quad 24$$

$$Lost\ Cl^- \text{ attr. to } A = [A] \cdot y_A \cdot \frac{MW_{Cl^-}}{MW_A} \quad 25$$

$$Lost\ Cl^- \text{ attr. to excess acidic species} = \sum_{A=ExSO_4^{2-}, ExNO_3^-, oxalate_{bulk}} Lost\ Cl^- \text{ attr. to } A \quad 26$$

339

340 We first calculate the percentage of Cl^- originally in sea salt particles that has been displaced
 341 by acidic species (% Cl^- depletion; Eq. 16) to facilitate comparisons between our results and other
 342 studies. Subsequently, mass concentrations of displaced Cl^- are calculated using two approaches
 343 to explore the effects of accounting for non-sea salt sources of Na^+ : Approach 1 quantifies
 344 displaced Cl^- using derived mass concentrations of $ssNa^+$ (lost Cl^- ; Eq. 17), while Approach 2
 345 determines displaced Cl^- using bulk PILS Na^+ mass concentrations (lost Cl_{bulk}^- ; Eq. 18), thus
 346 assuming sea salt is the only source of Na^+ . Mass concentrations of lost Cl_{bulk}^- will always be
 347 greater than corresponding values of lost Cl^- , and differences between the two (lost Cl_{diff}^- ; Eq. 19)
 348 are used to assess the significance in accounting for non-sea salt sources of Na^+ when evaluating
 349 the extent of Cl^- depletion processes and their potential effects on atmospheric chemistry.



350 As mentioned above, acidic species are responsible for displacing Cl^- from sea salt particles.
351 However, only a subset of the bulk PILS mass concentrations of SO_4^{2-} and NO_3^- are available for
352 Cl^- depletion reactions, as (i) SO_4^{2-} is a naturally occurring component of sea salt and (ii) available
353 NH_4^+ will neutralize certain amounts of SO_4^{2-} and potentially NO_3^- , leaving them relatively
354 unreactive. Equations 20 – 23 determine mass concentrations of non-sea salt, unneutralized SO_4^{2-}
355 , and NO_3^- , which are added to bulk PILS mass concentrations of oxalate to quantify the amount
356 of excess acidic species (Eq. 24) available for displacing Cl^- from sea salt particles. Note that we
357 use oxalate here as a proxy variable to represent organic acids in general as it is typically the most
358 abundant organic acid in tropospheric aerosol particles (e.g., Hilario et al., 2021; Ziemba et al.,
359 2011; Cruz et al., 2019). We calculate the theoretical amount of lost Cl^- attributable to each excess
360 acidic species (Eq. 25) as well as the total amount attributed to all measured excess acidic species
361 (Eq. 26). Results from Eq. 26 can be compared to values from Eq. 17 to identify the amount of lost
362 Cl^- explained by the measured excess acidic species, and discrepancies in these values may indicate
363 there are additional species contributing to Cl^- depletion (e.g., weak organic acids [Laskin et al.,
364 2012]; reactions initiated by O_3 [Keene et al., 1990]).

365 **2.5 MERRA-2 and NAAPS reanalysis products**

366 Wind speed and wind direction at 950 hPa were obtained from the Modern-Era Retrospective
367 Analysis for Research and Application, Version 2 (MERRA-2; Gelaro et al., 2017) to provide
368 context for large-scale boundary layer wind patterns over the region during each season/category
369 and/or flights of interest. Monthly averages were attained for December 2021 and January,
370 February, March, May, and June 2022 at $0.5^\circ \times 0.625^\circ$ spatial resolution, while 3-hour averages
371 were acquired for periods pertinent to each transit flight as well as the case study flights discussed
372 in Sects. 3.2 and 3.7.1. Monthly averages for December 2021, January 2022, and February 2022
373 were combined and averaged to produce a single wind vector field representative of the December-
374 February category, while averages for March, May, and June 2022 are used to portray conditions
375 for the March, May, and June Bermuda categories, respectively. The 950 hPa pressure layer was
376 selected as this is the Falcon’s median pressure altitude during the Winter 2022 and Summer 2022
377 deployments.

378 We relied on the Navy Aerosol Analysis and Prediction System (NAAPS) to identify the
379 presence of surface-level dust and smoke over the region on selected days using images from the
380 Aerosol Modeling archive (<https://www.nrlmry.navy.mil/aerosol/>) for the “Eastern United States”
381 and “Tropical Atlantic.” We selected images at 1800Z for each day as this time is most relevant to
382 flights during the Winter 2022 and Summer 2022 deployments. NAAPS surface dust and smoke
383 mass concentrations are gridded reanalysis products available at $1^\circ \times 1^\circ$ spatial resolution and 6-
384 hourly temporal resolution, where simulations of dust depend on surface erodible fraction and
385 surface friction velocity (Lynch et al., 2016), and those of smoke depend on size and duration of
386 satellite-detected hotspots (Reid et al., 2009; Hyer et al., 2013). Modeled atmospheric transport of
387 dust and smoke particles is then governed by the Navy Global Environmental Model (NAVGEM;
388 Hogan et al., 2014). These products are used to explore how influence from dust and smoke plumes
389 may affect calculations of Cl^- depletion for case studies presented in Sect. 3.7.1.

390

391 **3. Results and discussion**

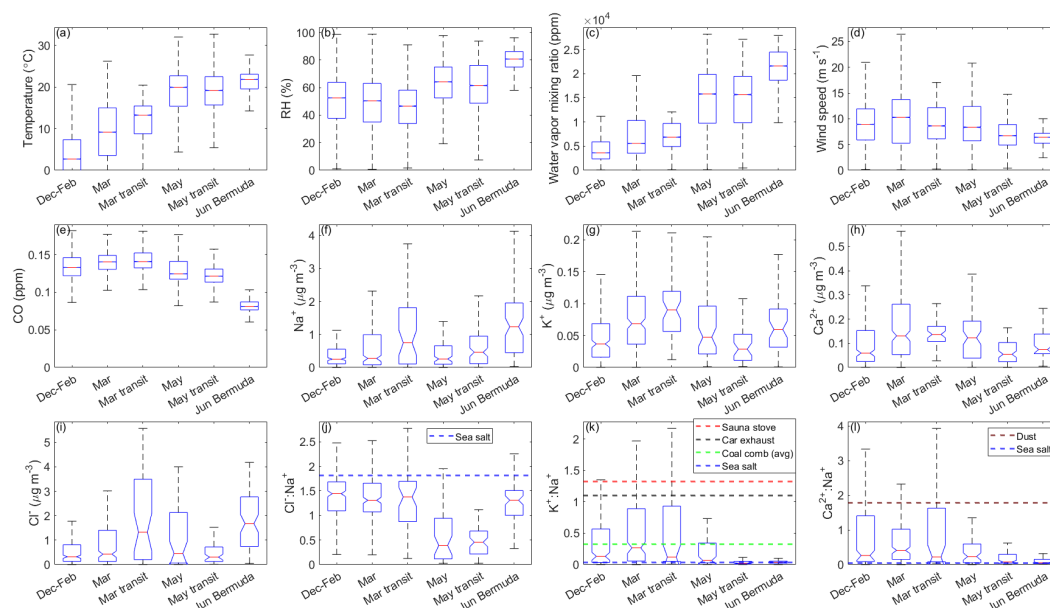
392 **3.1 Meteorological context**



393 Meteorological conditions during the Winter 2022 and Summer 2022 deployments are mostly
394 consistent with climatological characteristics reported for the NWA in Sorooshian et al. (2020)
395 and Painemal et al. (2021). Median temperatures are lowest in December-February (2.7°C)
396 followed by March (9.2°C), March transit (13.3°C ; recall the March transit flights are in late
397 March), May transit (19.2°C), May (19.9°C), and June Bermuda (21.9°C ; Fig. 1). Median water
398 vapor mixing ratios and RH follow the same trend with the exception that RH slightly decreases
399 from December-February (53%) to March (50%) and March transit (47%). Median wind speeds
400 are highest for March (10.3 m s^{-1}), similar for December-February, March transit, and May (8.9,
401 8.6, and 8.4 m s^{-1} , respectively), and lowest for May transit and June Bermuda (6.7 and 6.4 m s^{-1} ,
402 respectively). MERRA-2 wind fields at 950 hPa (e.g., Fig. 2) show westerly flow along the USEC
403 for December-February that transitions to southwesterly flow for March and March transit, which
404 is a typical progression as the Bermuda High begins to strengthen (Davis et al., 1997). For May
405 and May transit, zonal flow returns north of 34°N while relatively weak southwesterly flow
406 persists to the south. Southwesterly winds dominate for June Bermuda, and large-scale flow
407 patterns across the NWA appear conventional for a fully developed summertime Bermuda High.

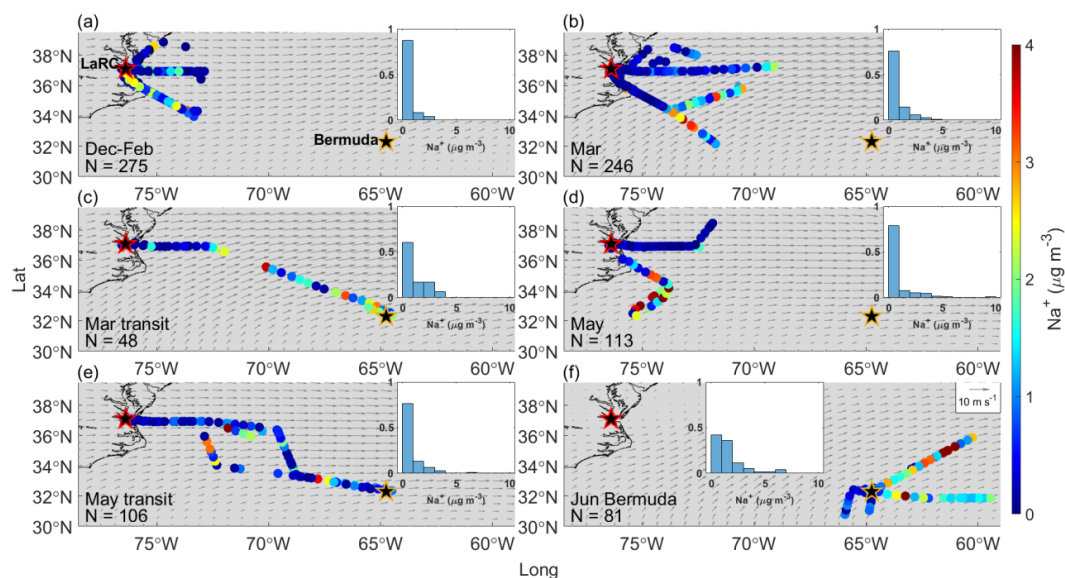
408 Median CO volume mixing ratios are highest for categories sampling solely along the USEC
409 (i.e., December-February [133 ppb], March [141 ppb], and May [124 ppb]) compared to June
410 Bermuda (81 ppb), affirming sampled coastal air masses were most influenced by anthropogenic
411 emissions. We refrain from using CO to compare levels of anthropogenic influence between
412 categories focused on the USEC as CO exhibits seasonal dependence over the NWA (Buchholz et
413 al., 2021). Specifically, peak values are typically observed in early spring due to wintertime
414 accumulation caused by reduced destruction by OH, while increased rates of oxidation by OH over
415 summer lead to minimum concentrations in late summer.

416 Precipitation is considered in this work as (i) wet scavenging processes remove sea salt
417 particles more efficiently than several other particle types (Galloway et al., 1993), and (ii) strong
418 winds associated with precipitation events can enhance sea salt emissions and offset scavenging
419 losses (Dadashazar et al., 2021; Grandey et al., 2011), both of which can influence the amount of
420 Cl^{-} available for depletion reactions on shorter time scales than the seasonal factors discussed
421 above. The NWA receives the most rainfall from December – February followed by June – August,
422 with precipitation rates peaking along the Gulf Stream in all seasons (Painemal et al., 2021).
423 Hawcroft et al. (2012) showed that 65 – 80% and 50 – 70% of the rainfall over the NWA in
424 December – February and June – August, respectively, is associated with midlatitude cyclones
425 (MLC)s, a common year-round weather phenomenon for the region (e.g., Braun et al., 2021;
426 Eichler and Higgins, 2006) largely dictating the eastward transport of trace gases and particulates
427 from North America to the adjacent marine environment (Keim et al., 2005; Cooper et al., 2002,
428 2001). Despite their frequency and known effects on other aerosol properties (e.g., aerosol optical
429 depth and size distribution; Grandey et al., 2011), there is uncertainty in how frontal passages
430 influence parameters relevant to Cl^{-} depletion over the NWA. During this study, meteorological
431 conditions were often driven by MLCs, with synoptic conditions changing every few days (Table
432 2). We discuss key variables in the context of prefrontal and postfrontal airstreams associated with
433 MLCs to explore the influence of midlatitude weather disturbances on depletion reactions and Cl
434 radical budgets over the NWA. Finally, note that clear-ensemble data for December-February do
435 not extend eastward of $\sim 73^{\circ}\text{W}$ due to frequent cloud cover below 3 km over the ocean. This should
436 be taken into consideration when comparing results for December-February to other categories,
437 especially for continentally sourced properties and/or those that depend on wind fetch.



438

439 **Figure 1.** Notched box plots showing seasonal/categorical differences in (a) temperature, (b)
 440 relative humidity (RH), (c) water vapor mixing ratio, (d) wind speed, (e) carbon monoxide (CO)
 441 mixing ratios, bulk mass concentrations from a particle into liquid sampler (PILS) of (f) chloride
 442 (Cl^-), (g) sodium (Na^+), (h) potassium (K^+), and (i) calcium (Ca^{2+}), as well as ratios of these mass
 443 concentrations for (j) $\text{Cl}^-:\text{Na}^+$, (k) $\text{K}^+:\text{Na}^+$, and (l) $\text{Ca}^{2+}:\text{Na}^+$. Data are from clear ensembles only.
 444 Typical ratios for particular ions in sea salt and/or dust are marked with dashed lines in j, k, and l.
 445 In k, we use additional lines to indicate ratios of $\text{K}^+:\text{Na}^+$ reported in the literature for inefficient
 446 batch combustion in a sauna stove (1.33; Lamberg et al., 2011), car exhaust (1.1; Huang et al.,
 447 1994), and coal combustion (0.33; Ondov et al., 1989). The solid red line in the center of each box
 448 indicates the median, box edges represent the 25th and 75th percentiles, and the lower and upper
 449 whiskers indicate the lower limit (first quartile - $1.5 \times$ interquartile range) and upper limit (third
 450 quartile + $1.5 \times$ interquartile range), respectively. The notches span the 95th confidence interval
 451 for the median.



452

453 **Figure 2.** Bulk PILS Na^+ mass concentrations from clear ensembles during (a) December 2021-
454 February 2022, (b) March 2022, (c) March 2022 transit flights between NASA Langley Research
455 Center (LaRC; marked with a red-edged star) and Bermuda (marked with a golden-edged star), (d)
456 May 2022, (e) May 2022 transit flights between LaRC and Bermuda, and (f) the Bermuda field
457 campaign in June 2022. Normalized histograms in each panel show the distribution of bulk PILS
458 Na^+ mass concentrations for that specific category since overlap among the colored dots can hide
459 some from view. Grey arrows indicate the average magnitude and direction of winds at 950 hPa
460 from MERRA-2 for the period relevant to each category.



461 **Table 2.** Dates, sample quantities, meteorological conditions, and aerosol particle properties
 462 relevant to Cl⁻ depletion for research flights (RFs) considered in each category. Median values of
 463 Na⁺_{bulk} and Ca²⁺_{bulk} are based on bulk PILS data while values of lost Cl⁻, Cl⁻ depletion, and excess
 464 acidic species are derived using Eqs. 1 – 5, 16, 17, and 20 - 24. "N PILS samples" refers to the
 465 total number of PILS samples collected during clear ensembles on the date indicated, while "N_{PILS}"
 466 refers to the number of these samples providing enough information to determine a given property.
 467 "N_{PILS&AMS}" refers to the number of coinciding mass concentrations from the PILS and aerosol
 468 mass spectrometer (AMS) necessary for calculating excess acidic species mass concentrations.

Category	Date	RF(s)	N PILS samples	Meteorological conditions and/or relevant notes	Na ⁺ _{bulk}		Ca ²⁺ _{bulk}		Lost Cl ⁻		Cl ⁻ depletion		Excess acidic species	
					Median (µg m ⁻³)	N _{PILS}	Median (µg m ⁻³)	N _{PILS}	Median (µg m ⁻³ /pptv)	N _{PILS}	Median (%)	N _{PILS}	Median (µg m ⁻³)	N _{PILS & AMS}
Dec-Feb	30 November 2021	94	7	Remains of post-frontal conditions	0.14	7	0.31	7	-0.17/NA ¹	7	0	7	0.29	13
	01 December 2021	95	16	Prefrontal, high pressure; smoke in boundary layer near coast	0.30	16	0.49	16	-0.16/NA ¹	16	0	16	0.59	136
	07 December 2021	96	5	Postfrontal, cold high pressure behind a strong cold front	0.19	5	0.20	5	-0.12/NA ¹	5	0	5	0.03	22
	11 January 2022	100, 101	6	Cold high pressure, cold air outbreak (CAO) conditions	0.34	4	0.05	6	0.12/80	4	20	4	0.49	21
	12 January 2022	102, 103	33	Cold high pressure	0.21	29	0.06	21	0.01/7	15	4	15	0.20	109
	15 January 2022	104	3	Postfrontal	0.63	3	0.05	2	0.01/7	2	4	2	0.35	20
	18 January 2022	105	11	Low pressure moves offshore, sets up CAO conditions	0.22	2	0.06	2	NaN	0	NaN	0	0.01	10
	19 January 2022	107, 108	26	Short-lived high pressure	0.24	14	0.06	10	-0.05/NA ¹	6	0	6	0.14	66
	24 January 2022	109, 110	26	Postfrontal, weak high pressure	0.07	15	0.03	13	-0.04/NA ¹	8	0	8	0.02	86
	26 January 2022	111, 112	20	Postfrontal	0.12	12	0.03	10	0.00/0	7	0	7	0.01	83
	27 January 2022	113, 114	18	Cold high pressure	0.25	16	0.01	5	0.06/40	5	21	5	0.36	41
	01 February 2022	115	8	High pressure	0.90	6	0.05	7	0.41/273	5	21	5	1.00	37
	02 February 2022	116	17	High pressure	0.73	16	0.03	6	0.18/120	6	12	6	0.41	44
	03 February 2022	117, 118	15	High pressure	1.03	14	0.03	5	0.04/27	5	2	5	0.00	10
	15 February 2022	120, 121	34	Postfrontal conditions, cold high pressure	0.25	27	0.03	24	0.08/53	21	17	21	0.56	69
	16 February 2022	122, 123	21	Cold high pressure	0.20	18	0.08	20	0.10/67	16	27	16	0.53	105
19 February 2022	124, 125	38	Weak postfrontal	0.12	30	0.06	37	0.06/40	23	24	23	0.24	186	



	22 February 2022	126, 127	25	Prefrontal, high pressure	1.41	25	0.12	24	0.45/300	24	17	24	0.64	184
	26 February 2022	128, 129	16	Postfrontal	0.13	16	0.06	15	-0.02/NA ¹	15	0	15	0.27	130
	Overall		345		0.25	275	0.06	235	0.04/27	190	6	190	0.30	1372
Mar	02 March 2022	130	39	Postfrontal, high pressure	0.30	36.00	0.16	39	0.04/27	33	8	33	1.20	298
	03 March 2022	131, 132	71	Weak prefrontal	0.91	57.00	0.27	71	0.10/67	57	9	57	1.19	537
	04 March 2022	133, 134	42	Cold high pressure	1.56	40.00	0.12	39	0.42/280	36	14	36	1.02	242
	13 March 2022	138	8	Postfrontal, CAO conditions	0.12	6.00	0.06	7	-0.12/NA ¹	6	0	6	0.02	22
	14 March 2022	139, 140	38	Late postfrontal, cold high pressure; smoke plume sampled from a woodland fire	0.16	37.00	0.06	37	0.03/20	35	13	35	0.22	305
	18 March 2022	141	14	Weak postfrontal	0.18	14.00	0.04	12	0.05/33	12	35	12	0.33	98
	26 March 2022	144, 145	29	Postfrontal; sampled dust, smoke, and potentially pollen	0.05	22.00	0.04	22	-0.02/NA ¹	13	0	13	0.00	147
	28 March 2022	146	17	Postfrontal	0.07	17.00	0.05	12	-0.01/NA ¹	10	0	10	0.13	98
	29 March 2022	147, 148	19	Postfrontal, high pressure, CAO conditions	0.21	17.00	0.05	5	0.02/13	4	34	4	0.00	43
	Overall		277		0.27	246	0.13	244	0.04/27	206	10	206	0.57	1790
May	03 May 2022	149	15	Weak prefrontal; presence of smoke potentially from New Mexico	0.42	15	0.14	12	0.89/594	7	85	7	0.03	92
	05 May 2022	150, 151	18	Postfrontal	0.05	14	0.04	14	0.42/280	2	89	2	0.02	91
	16 May 2022	153, 154	39	Prefrontal to an approaching cold front yet also postfrontal to a departing band of precipitation	0.26	39	0.26	7	0.65/434	1	73	1	0.05	85
	17 May 2022	155	37	Postfrontal	0.08	17	0.01	13	1.53/1020	2	73	2	0.05	52
	20 May 2022	158	28	Warm high pressure, southerly flow due to Bermuda high ² ; haze with potential sampling of bioaerosol	1.75	28	0.17	27	1.91/1274	21	48	21	0.97	148
	Overall		137		0.26	113	0.12	73	1.76/1174	33	64	33	0.05	468
Mar transit	22 March 2022	142, 143	48	High pressure, two days after a cold front and two days before another cold front	0.75	48	0.14	48	0.11/73	43	9	43	0.36	423
May transit	18 May 2022	156, 157	67	Postfrontal along East Coast, aircraft passed across the cold front on the way to Bermuda	0.51	58	0.05	50	1.37/914	31	74	31	0.27	216



	21 May 2022	159, 160	42	Warm high pressure, anticyclonic flow around Bermuda high	0.50	37	0.08	26	1.67/1114	17	75	17	1.87	137
	31 May 2022	161	11	Postfrontal	0.18	11	0.02	5	0.22/147	5	67	5	0.02	20
	Overall		120		0.46	106	0.05	81	1.33/887	53	74	53	0.44	373
Jun Bermuda	02 June 2022	162, 163	4	Prefrontal	0.64	4	0.03	3	0.71/474	2	44	2	2.62	12
	03 June 2022	164	1	Prefrontal, tropical system approaching from the southwest	0.30	1	NaN	0	NaN	0	NaN	0	0.02	1
	05 June 2022	165	29	Could only fly in the morning due to approaching tropical cyclone (TC), TC departs 06 June 2022.	1.76	29	0.08	26	1.35/900	26	36	26	1.97	213
	07 June 2022	167	1	High behind departing TC	2.21	1	NaN	0	NaN	0	NaN	0	0.02	1
	08 June 2022	168, 169	2	High pressure behind TC, African dust known to be in domain	4.28	2	1.07	1	1.12/747	1	11	1	0.04	9
	10 June 2022	170	1	High pressure, isolated thunderstorms, African dust known to be in domain	2.28	1	0.06	1	0.68/454	1	17	1	1.19	9
	11 June 2022	172, 173	20	High pressure, African dust known to be in domain	0.33	20	0.21	12	0.15/100	11	11	11	1.12	71
	13 June 2022	174	25	High pressure, African dust known to be in domain but sampled away from dust for contrast	1.34	23	0.06	24	0.48/320	23	17	23	1.89	170
	Overall		83		1.24	81	0.07	67	0.66/440	64	25	64	1.82	486

469 ¹Negative mass concentrations in $\mu\text{g m}^{-3}$ are reported for lost Cl^- and can be conceptualized as the
 470 amount of measured particulate Cl^- in excess of what would be in unreacted sea salt particles based
 471 on Eqs. 1 – 4. Negative values may suggest there are additional non-sea salt sources of particulate
 472 Cl^- within the sampled air mass. In these cases, we do not provide corresponding gas phase
 473 concentrations of lost Cl^- in pptv as these are only meaningful when Cl^- is displaced from sea salt
 474 particles.

475 ²Davis et al. (1997)



476 **3.2 Seasonal, spatial, and frontal trends in Na⁺**

477 Cl⁻ depletion studies are motivated by the fact that radicals produced via depletion reactions
478 can influence atmospheric chemistry, the extent to which largely depends on the quantity of
479 radicals generated. Therefore, the amount of Cl⁻ in sea salt available to depletion reactions is
480 critical to quantify, which is why a large portion of our initial discussion is about trends in bulk
481 Na⁺ mass concentrations as they are a reliable indicator of sea salt mass concentrations. Bulk PILS
482 Na⁺ mass concentrations are remarkably similar for December-February, March, and May (median
483 mass concentrations of 0.25, 0.27, and 0.26 $\mu\text{g m}^{-3}$, respectively), higher for March transit and
484 May transit (0.75 and 0.46 $\mu\text{g m}^{-3}$, respectively), and highest in and around Bermuda (1.24 $\mu\text{g m}^{-3}$).
485 In general, past works also typically report higher sea salt mass concentrations in open-ocean
486 environments compared to coastal locations (Table S4), which is intuitive considering that wind
487 fetch is one important factor governing atmospheric sea salt mass concentrations. However, if Na⁺
488 mass concentrations were dictated chiefly by wind fetch over the NWA, values would mostly
489 increase moving eastward, which is not always the case (e.g., Fig. 2e). In fact, there does not appear
490 to be any distinct spatial gradients in Na⁺ mass concentrations for the seasons/categories presented,
491 yet (i) overlap of flight tracks makes it difficult to view all mass concentrations at once, and (ii)
492 we do not have enough data to state that this is always true for the region.

493 Aside from wind fetch, removal via wet scavenging processes is another factor dictating sea
494 salt mass concentrations over marine environments. We explore the effect of passing frontal
495 systems on bulk Na⁺ mass concentrations for December-February, March, and May as (i) bulk Na⁺
496 appears seasonally independent among these categories and (ii) flights sampled the same general
497 region, allowing us to remove coastal versus open-ocean sampling as a confounding variable.
498 When applying the meteorological conditions identified for each day in Table 2, bulk Na⁺ mass
499 concentrations are generally higher during prefrontal/high pressure conditions compared to
500 postfrontal scenes for each seasonal/monthly category (Fig. 3). It is not unusual for bulk Na⁺ mass
501 concentrations to exceed 3 $\mu\text{g m}^{-3}$ in prefrontal and/or high-pressure conditions, especially in
502 March and May, yet values never exceed this threshold in postfrontal conditions. Although bulk
503 statistics suggest frontal passages may reduce sea salt mass concentrations over the NWA, data
504 from prefrontal and postfrontal conditions are not guaranteed to be linked, meaning samples
505 quantifying bulk Na⁺ before and after each frontal passage are not always available. Therefore, we
506 isolate bulk Na⁺ mass concentrations for flights straddling frontal passages to assess the
507 relationship of sea salt mass concentrations and MLCs on a case-study level.

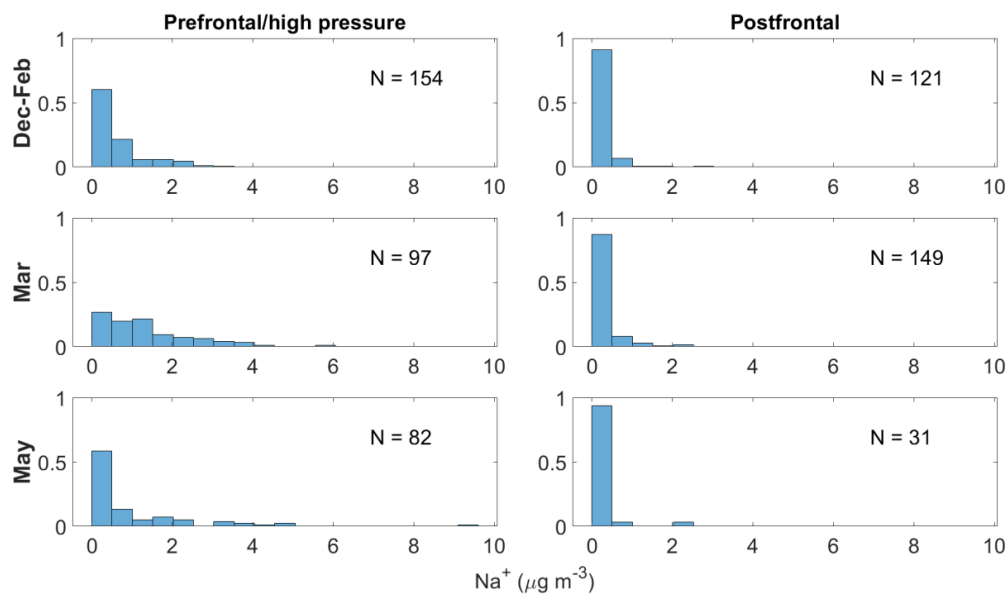
508 Postfrontal conditions on 19 February 2022 (RFs 124 and 125) are associated with bulk Na⁺
509 mass concentrations mostly < 0.3 $\mu\text{g m}^{-3}$ and moderate westerly winds bringing continental air
510 over the NWA (Fig. S1). Three days later (22 February 2022; RFs 126 and 127), prefrontal
511 conditions show increased bulk Na⁺ mass concentrations that are distributed evenly from 0.3 – 2.7
512 $\mu\text{g m}^{-3}$ and southerly winds along the coast. Bulk Na⁺ mass concentrations then swiftly decrease
513 to values mostly below 0.3 $\mu\text{g m}^{-3}$ by 26 February 2022 (RFs 128 and 129) as another MLC moves
514 through the region, although note clear-ensemble sampling was more restricted to the coastline on
515 this day compared to 19 and 22 February 2022.

516 Unfortunately, samples straddling a frontal passage for March are unavailable, but we use
517 consecutive flights from 02 – 04 March 2022 to depict the “recharge” of sea salt mass
518 concentrations following a MLC (Fig. S2). Bulk Na⁺ mass distributions gradually shift towards
519 larger mass concentrations moving from postfrontal conditions with gentle westerly winds (02
520 March 2022; RF 130), to weak prefrontal conditions with stronger northwesterly and southwesterly
521 winds converging at 36 °N (03 March 2022; RFs 131 and 132), and, finally, to cold high-pressure



522 conditions with moderate anticyclonic flow around a high over the northeastern U.S. (04 March
523 2022; RFs 133 and 134). Air masses sampled on 02 and 03 March 2022 appear more continentally
524 influenced and may have been more recently affected by large-scale precipitation compared to the
525 marine air mass sampled on 04 March 2022, which is a potential explanation for the differences in
526 bulk Na^+ mass concentrations.

527 Flights on 16 May 2022 (RFs 153 and 154) sampled an air mass recently impacted by a
528 retreating band of precipitation yet also considered as prefrontal due to an approaching cold front
529 (Fig. S3). As there was limited time for sea salt mass concentrations to recharge between the
530 consecutive MLCs, it is unsurprising there is little difference in bulk Na^+ mass concentrations
531 between 16 May 2022 and the postfrontal conditions sampled on 17 May 2022 (RF 155). Frontal
532 influence dissipated by 20 May 2022 (RF 158) with southwesterly flow returning along the
533 coastline in association with the strengthening Bermuda High. This, and the absence of
534 precipitation for several days, may help explain the increase in bulk Na^+ mass concentrations from
535 mostly below $1 \mu\text{g m}^{-3}$ on 16 – 17 May 2022 to a mostly above this value on 20 May 2022. The
536 three case studies presented are meant to illustrate how rapidly sea salt mass concentrations can
537 change over the NWA due, in part, to fluctuations in synoptic-scale wind patterns and/or large-
538 scale precipitation associated with MLCs. However, we acknowledge that there are many other
539 confounding atmospheric variables influencing sea salt mass concentrations during these case
540 studies and that flight tracks do not cover the exact same locations on each of these days. Although
541 we do not have enough data to make definitive claims, bulk statistical and case study analyses
542 suggest sea salt mass concentrations decrease behind passing MLCs over the NWA, which
543 corresponds to reduced potential in the amount of reactive chlorine-containing gases that could be
544 produced via depletion reactions compared to in prefrontal and high-pressure conditions.



545

546 **Figure 3.** Normalized histograms showing differences in bulk PILS Na^+ mass concentrations from
547 clear ensembles occurring in prefrontal and/or high-pressure versus postfrontal conditions for
548 December-February (top row), March (middle row), and May (bottom row). These categories are
549 shown as they represent flights occurring in and around the East Coast, eliminating coastal versus
550 open-ocean sampling as a confounding variable.



551 **3.3 Seasonal trends in K⁺, Ca²⁺, Cl⁻ and ion mass ratios**

552 As described above, the NWA receives BB emissions from continuous sources (e.g.,
553 fossil fuel combustion for transportation and industrial efforts along the USEC), seasonal practices
554 (e.g., agricultural waste burning in spring, wood burning in winter), and intermittent yet influential
555 events (e.g., forest fires). Using K⁺ as a tracer for such activities, BB influence is greatest during
556 March and March transit flights with median bulk K⁺ mass concentrations of 0.07 and 0.09 μg m⁻³,
557 respectively, compared to 0.04, 0.05, 0.03 and 0.06 μg m⁻³ for the December-February, May,
558 May transit, and June Bermuda categories, respectively. This agrees with previous findings where
559 mass concentrations of organic carbon and particles with diameters 2.5 – 10 μm (PM_{coarse}) were
560 much higher in March than in any other month at a coastal site in Florida (Edwards et al., 2021),
561 and this was attributed mostly to the annual peak in prescribed burning across the southeastern
562 U.S. (Jaffe et al., 2020; McCarty et al., 2007). Our bulk K⁺ mass concentrations are comparable to
563 mean values reported at a receptor site for BB and urban emissions from East Asia (0.02 – 0.05 μg
564 m⁻³; Boreddy and Kawamura, 2015) as well as those in polluted air masses containing dust (0.03
565 μg m⁻³) and biogenically influenced air masses (0.03 μg m⁻³) over the southeastern U.S. during the
566 Study of Emissions and Atmospheric Composition, Clouds, and Climate Coupling by Regional
567 Surveys (SEAC⁴RS; Kacenelenbogen et al., 2022). However, bulk K⁺ values are mostly lower than
568 average K⁺ mass concentrations in air masses influenced by agricultural burning (0.10 μg m⁻³) and
569 wildfire emissions (0.09 μg m⁻³) during SEAC⁴RS (Kacenelenbogen et al., 2022) and also lower
570 than average mass concentrations (0.82 μg m⁻³) measured during the Fire Influence on Regional to
571 Global Environments and Air Quality (FIREX-AQ) airborne field campaign (Adachi et al., 2022)
572 sampling BB plumes in the western and southeastern U.S. Thus, BB particles were consistently
573 present during the Winter 2022 and Summer 2022 deployments, yet relatively dilute compared to
574 their levels in air masses more heavily influenced by BB processes. This is an important point to
575 consider when contemplating how BB emissions may affect estimates of Cl⁻ depletion, which is
576 discussed in greater detail in Sect. 3.7.2.

577 We use bulk Ca²⁺ to identify influence from dust particles and see a similar trend as above
578 where median bulk Ca²⁺ mass concentrations are higher in certain spring categories (0.13, 0.14,
579 and 0.12 μg m⁻³ for the March, March transit, and May categories, respectively) compared to
580 December-February (0.06 μg m⁻³) and June Bermuda (0.07 μg m⁻³). Higher springtime bulk Ca²⁺
581 mass concentrations are likely due to periodic influence from Asian dust plumes, which arrive
582 most frequently over the region from March-May (Aldhaif et al., 2020), and/or to increased
583 suspension of dust particles in BB plumes from agricultural fires across the eastern and
584 southeastern U.S. due to turbulent mixing around flames and the burn front (e.g., Kavouras et al.,
585 2012; Popovicheva et al., 2014; Maudlin et al., 2015; Schlosser et al., 2017; Palmer, 1981).
586 Interestingly, bulk Ca²⁺ mass concentrations are lowest for May transit (0.05 μg m⁻³), but this may
587 be explained by the episodic nature of dust events over the NWA (e.g., Wu et al., 2015; Perry et
588 al., 1997; Prospero, 1999) and the fact that this category is comprised of only three days. African
589 dust plumes become more common over the NWA from June-August (Zuidema et al., 2019) with
590 the strengthening of the Bermuda High, yet the Summer 2022 deployment ended just as these
591 plumes were becoming evident over the region (see meteorological notes for 10, 11, and 13 June
592 2022 in Table 2). There does not appear to be distinct spatial trends in bulk Ca²⁺ over the region
593 for most categories (Fig. S4), presumably as fluctuations in bulk Ca²⁺ may be largely driven by
594 periodic influence from long-range dust transport, smoke plumes from fires along the USEC
595 advecting over the ocean, and midlatitude weather disturbances (Fig. S5). However, a gradient
596 seems to exist along the March transit flights (RFs 142 and 143 on 22 March 2022) such that bulk



597 Ca^{2+} mass concentrations are highest to the east of LaRC and then decrease to the southeast
598 towards Bermuda. This potential sampling of a dust plume and its implications on calculations
599 relevant to Cl^- depletion are explored further in Sect. 3.7.1.

600 Median Cl^- mass concentrations exhibit slightly different seasonal trends than bulk Na^+ , with
601 values lowest for May transit ($0.31 \mu\text{g m}^{-3}$), slightly higher for December-February, March, and
602 May (0.32 , 0.43 , and $0.46 \mu\text{g m}^{-3}$, respectively), and much higher for March transit and Bermuda
603 (1.33 and $1.68 \mu\text{g m}^{-3}$, respectively). The fact that May transit has the third highest median bulk
604 Na^+ mass concentration yet the lowest Cl^- median is the main difference in seasonal trends between
605 these species, which may seem to suggest Cl^- depletion processes are most active for May transit.
606 However, the number of PILS samples providing (i) bulk Na^+ and (ii) Cl^- mass concentrations are
607 very different for May (113 and 43, respectively) and May transit (106 and 65, respectively), yet
608 comparable for December-February, March, March transit, and June Bermuda (Table S5). Thus,
609 it is best to avoid drawing conclusions about Cl^- depletion from individual trends in bulk Na^+ and
610 Cl^- , and to instead focus on samples providing mass concentrations for both species. These samples
611 were isolated to generate the statistics shown in Fig. 1j, which (i) can be considered as a precursory
612 analysis for Cl^- depletion over the NWA where sea salt is assumed to be the only source of Na^+ ,
613 and (ii) are directly comparable to many past works making this assumption. Ratios of $\text{Cl}^-:\text{Na}^+$ are
614 below 1.81 for all categories, suggesting Cl^- depletion processes are consistently occurring over
615 the region. However, median values are much lower for May (0.39) and May transit (0.46)
616 compared to December-February (1.44), March (1.31), March transit (1.38), and June Bermuda
617 (1.31), suggesting that depletion reactions are particularly prevalent in late spring. May and May
618 transit ratios are comparable to those previously reported along the USEC (Quinn and Bates, 2005;
619 Nolte et al., 2008; Zhao and Gao, 2008) in late spring and summer, especially for submicron sea
620 salt particles.

621 As mentioned above, $\text{Cl}^-:\text{Na}^+$ ratios are only an appropriate means to illustrate the extent of Cl^-
622 depletion if sea salt is the predominant source of each species. Ratios of bulk $\text{K}^+:\text{Na}^+$ and $\text{Ca}^{2+}:\text{Na}^+$
623 are useful for indicating if other particle types may be contributing to bulk Na^+ concentrations as
624 these ions are present in distinctly different proportions in sea salt, emissions from various
625 combustion processes, and dust particles. Combustion and/or BB activities do not appear to
626 contribute meaningfully to bulk Na^+ for May, May transit, and June Bermuda as $\text{K}^+:\text{Na}^+$ ratios
627 (0.065 , 0.020 , and 0.037 , respectively) are fairly similar to the reference value for sea salt (0.036 ;
628 Seinfeld and Pandis, 2016; Finlayson-Pitts and Pitts, 2000), whereas ratios exceeding this value
629 are observed for December-February (0.132), March (0.267), and March transit (0.119). Table 2
630 indicates smoke was only directly sampled on four days of the Winter 2022 and Summer 2022
631 deployments (01 December 2021, 14 March 2022, 26 March 2022, and 03 May 2022), suggesting
632 increased $\text{K}^+:\text{Na}^+$ ratios for December-February, March, and March transit may have been driven
633 by increased background levels of BB particles over the NWA from widespread and continuous
634 residential wood burning and prescribed agricultural burning in winter and early spring as opposed
635 to acute BB events. All categories have median $\text{Ca}^{2+}:\text{Na}^+$ ratios exceeding the reference value for
636 sea salt (0.038 ; Bowen, 1979; Finlayson-Pitts and Pitts, 2000), with values of 0.412 , 0.261 , 0.233 ,
637 0.219 , 0.075 , and 0.050 for March, December-February, May, March transit, May transit, and June
638 Bermuda, respectively. These results nicely motivate an investigation into how estimates of Cl^-
639 depletion change when eliminating contributions of (i) dust and (ii) both dust and combustion
640 emissions to bulk Na^+ mass concentrations, which are the topics of Sects. 3.7.1 and 3.7.2,
641 respectively.

642



643 3.4 Seasonal, spatial, and frontal trends in acidic species

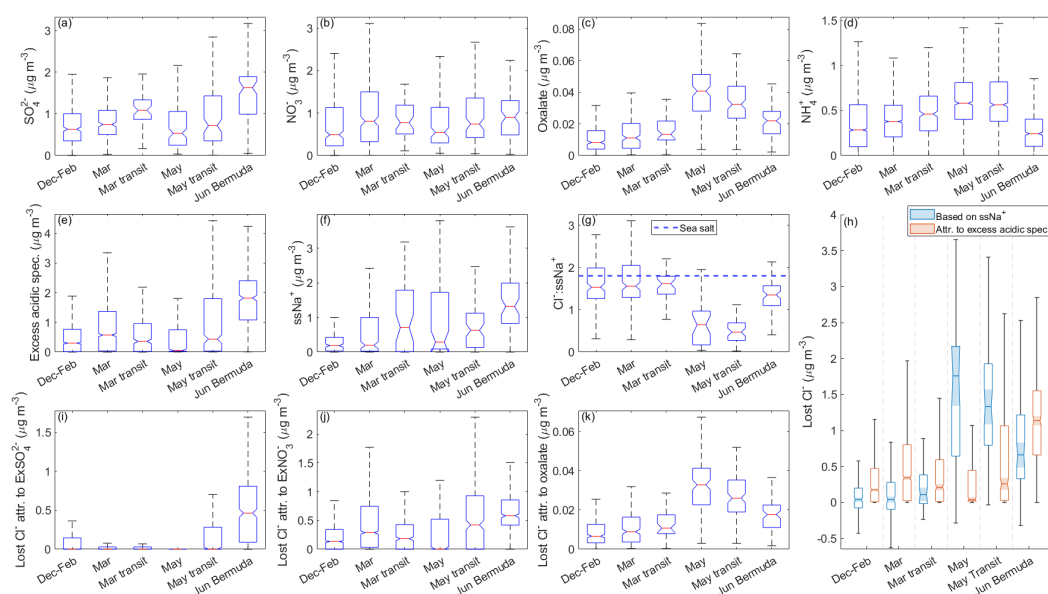
644 Sea salt mass concentrations alone control the maximum amount of reactive chlorine-
645 containing gases that can be released via Cl^- depletion reactions, but available acidic species are
646 an important factor in regulating the extent to which these reactive gases are actually released.
647 Median mass concentrations of bulk SO_4^{2-} show that this acidic species is a common constituent
648 of sampled air masses, especially for March transit and June Bermuda (Fig. 4; Table S6). Median
649 bulk NO_3^- mass concentrations are of similar magnitude to bulk SO_4^{2-} , yet exhibit less variability
650 among the categories, while oxalate is present in relatively low amounts for December-February,
651 March, and March transit, increases sharply for May and May transit, and then decreases slightly
652 for June Bermuda. In Sect. 2.4, we describe how ssNa^+ mass concentrations and subsequently
653 derived parameters can be calculated either by assuming (i) dust and sea salt or (ii) dust, sea salt,
654 and combustion-sourced particles contribute to bulk Na^+ . In this section and Sects. 3.5, 3.6, 3.7.1,
655 and 3.7.3, we discuss values based on the first assumption, whereas those based on the second
656 assumption are the topic of Sect. 3.7.2.

657 After accounting for contributions of sea salt to SO_4^{2-} and neutralization of non-sea salt SO_4^{2-}
658 and NO_3^- with NH_4^+ , excess SO_4^{2-} (ExSO_4^{2-}) is typically nonexistent for all categories except June
659 Bermuda (median of $0.63 \mu\text{g m}^{-3}$; Fig. S6), while a range of mass concentrations of excess NO_3^-
660 (ExNO_3^-) remain for all categories except May (0.24, 0.51, 0.32, 0.74, $1.02 \mu\text{g m}^{-3}$ for December-
661 February, March, March transit, May transit, and June Bermuda, respectively). Thus, mass
662 concentrations of measured acidic species available to participate in Cl^- depletion reactions are
663 relatively low for May ($0.05 \mu\text{g m}^{-3}$; contributed mostly by oxalate), moderate for December-
664 February, March, March transit, and May transit ($0.30, 0.57, 0.36, 0.44 \mu\text{g m}^{-3}$, respectively), and
665 relatively high for June Bermuda ($1.82 \mu\text{g m}^{-3}$). However, recall that oxalate is used in this study
666 as a proxy for general trends in organic acids, many of which have been shown to considerably
667 displace Cl^- from sea salt particles (e.g., Laskin et al., 2012), including formate, acetate, MSA, and
668 succinate (Kerminen et al., 1998; Braun et al., 2017); thus the results based on oxalate are a lower
669 bound for the effects organic acids have on depletion reactions. Although lower than other aerosol
670 constituents, oxalate mass concentrations are highest for May and May transit along with those of
671 m/z 44, a marker of oxygenated organics that has been shown to correlate with organic acids
672 (Zhang et al., 2005; Takegawa et al., 2007; Sorooshian et al., 2010), and m/z 79, a marker for MSA
673 (Zorn et al., 2008; Van Rooy et al., 2021). Median m/z 44 mass concentrations especially suggest
674 organic acids may play an important role in sea salt particle chemistry for May and May transit as
675 values (0.46 and $0.41 \mu\text{g m}^{-3}$, respectively) (i) are comparable to those of other dominant acidic
676 species over the region, (ii) represent the mass only of the particle fragments (i.e., carboxylic acids)
677 able to displace Cl^- , and (iii) reflect a lower limit of what is actually available for depletion
678 reactions as AMS measurements are for particles 60 – 600 nm.

679 Like sea salt mass concentrations, excess acidic species do not display clear zonal or
680 meridional trends over the NWA (Fig. S7) but do appear to decrease near the USEC following the
681 passage of MLCs (Fig. S8). The reasons are uncertain for such high mass concentrations of excess
682 acidic species for June Bermuda, but a probable cause may be emissions of DMS from marine
683 organisms oxidizing to produce H_2SO_4 (e.g., Luria et al., 1989; Andreae et al., 2003). Excess acidic
684 species mass concentrations are not nearly as high near Bermuda for March transit and May transit
685 compared to June Bermuda, suggesting the increased values in June may be (i) due to greater
686 photochemical production of SO_4^{2-} with increased incident solar radiation (Parungo et al., 1987;
687 Corral et al., 2021) or (ii) due to an episodic surge in local marine biological activity, which has
688 been shown to occur around Bermuda when higher doses of solar radiation become available to



689 the upper mixed layer of the ocean (Vallina and Simó, 2007; Toole and Siegel, 2004). Level-3 (8-
690 day average, 4 km resolution) sea surface chlorophyll a concentrations from MODIS-Aqua show
691 consistent values around Bermuda for March transit, May transit, and June Bermuda. However,
692 there is an important distinction between biomass and ocean biological activity such that steady
693 biomass around Bermuda does not necessarily correspond to similar gaseous emission rates for
694 these categories. Thus, additional research is needed to better understand the seasonal variations
695 in excess acidic species around Bermuda.



696

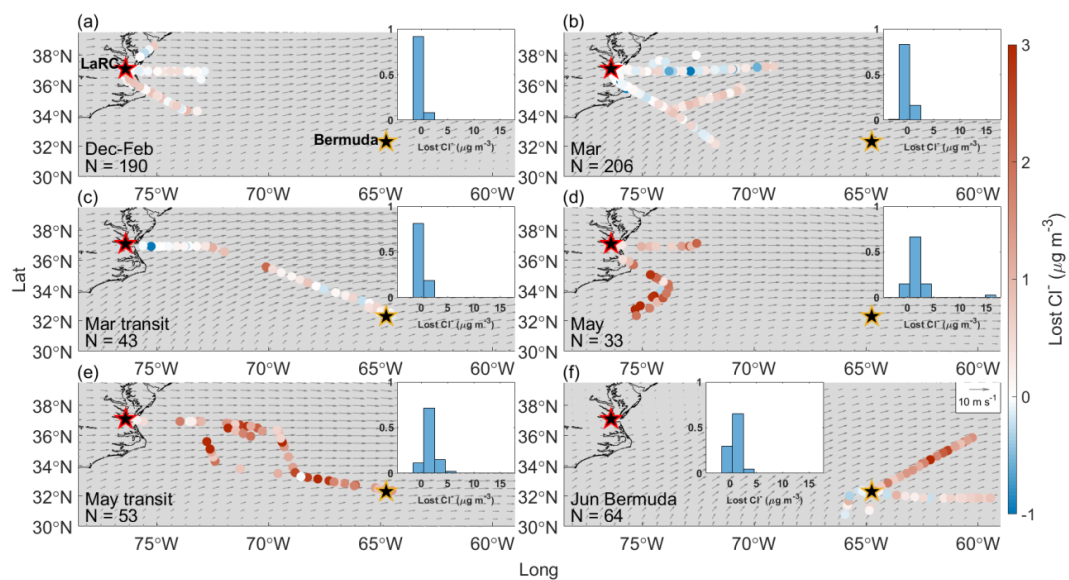
697 **Figure 4.** Notched box plots showing seasonal/categorical differences in observed mass
 698 concentrations from clear ensembles of bulk PILS (a) sulfate (SO_4^{2-}), (b) nitrate (NO_3^-), and (c)
 699 oxalate, as well as (d) AMS ammonium (NH_4^+). Similar plots are shown for derived mass
 700 concentrations of (e) total excess acidic species, (f) sea salt Na^+ (ssNa^+), the ratio of (g) $\text{Cl}^-:\text{ssNa}^+$,
 701 (h) mass concentrations of actual and theoretical lost Cl^- , as well as theoretical mass concentrations
 702 of lost Cl^- attributable to (i) excess SO_4^{2-} (ExSO_4^{2-}), (j) excess NO_3^- (ExNO_3^-), and (k)
 703 oxalate. The value of $\text{Cl}^-:\text{Na}^+$ in sea salt (1.81; Seinfeld and Pandis, 2016) is indicated in g with a horizontal
 704 dashed blue line. In h, light blue boxes represent the actual Cl^- displaced from sea salt particles
 705 based on derived mass concentrations of ssNa^+ , while light red boxes represent the theoretical
 706 amount of Cl^- that could have been displaced by the derived mass concentrations of excess acidic
 707 species. The properties of the boxes are the same as described in Fig. 1.



708 3.5 Seasonal, spatial, and frontal trends in Cl⁻ depletion

709 Median ssNa⁺ mass concentrations display similar trends to bulk Na⁺ with comparable values
710 among the December-February, March, and May categories (0.19, 0.20, and 0.29 μg m⁻³,
711 respectively), higher mass concentrations for March transit and May transit (0.71 and 0.63 μg m⁻³,
712 respectively), and highest values for June Bermuda (1.32 μg m⁻³). Median ratios of Cl⁻:ssNa⁺
713 (1.54, 1.56, 1.62, 0.65, 0.47, and 1.35 for December-February, March, March transit, May, May
714 transit, and June Bermuda, respectively) are higher than those of Cl⁻:Na⁺ for each category, serving
715 as a preliminary example of how neglecting contributions of dust to bulk Na⁺ can lead to
716 overestimates of Cl⁻ depletion. Regardless of magnitude, Cl⁻:Na⁺ and Cl⁻:ssNa⁺ ratios both convey
717 that the greatest fraction of available sea salt Cl⁻ is converted to reactive chlorine-containing gas
718 during the month of May (i.e., May and May transit categories) over the NWA. Lost Cl⁻ mass
719 concentrations are relatively low for December-February, March, and March transit (0.04, 0.04,
720 and 0.11 μg m⁻³, respectively) then abruptly increase for May and May transit (1.76 and 1.33 μg
721 m⁻³, respectively) followed by a moderate decrease for June Bermuda (0.66 μg m⁻³). These mass
722 concentrations correspond to increases in atmospheric mixing ratios of reactive chlorine-
723 containing gas of 27, 27, 73, 1174, 887, and 440 pptv, respectively, suggesting Cl⁻ depletion
724 processes have the potential to considerably alter rates of boundary layer VOC oxidation in May
725 over the NWA; recall that Singh and Kasting [1998] reported ppbv levels of such gases can
726 produce enough Cl radicals to oxidize 20 – 40% of tropospheric nonmethane alkanes. However,
727 note our reported lost Cl⁻ mass concentrations are for particles with diameters < 5 μm, so although
728 May appears to be the only category where Cl⁻ depletion is severe enough to potentially accelerate
729 tropospheric VOC oxidation, lost Cl⁻ mass concentrations may be higher in reality for other
730 categories, depending on the extent of depletion reactions in larger sea salt particles.

731 There is not a clear spatial gradient in lost Cl⁻ over the region (Fig. 5), but mass concentrations
732 decrease near the USEC after passing frontal systems (Fig. S9), both of which are intuitive as bulk
733 Na⁺ and excess acidic species mass concentrations display the same trends. Although median lost
734 Cl⁻ mass concentrations are above 0 for all categories, negative lost Cl⁻ mass concentrations are
735 observed in 45, 42, 35, 3, 2, and 14% of the samples for December-February, March, March transit,
736 May, May transit, and June Bermuda, respectively. Negative lost Cl⁻ values can be interpreted as
737 there being more Cl⁻ in a sample than expected for unreacted sea salt particles based on derived
738 mass concentrations of ssNa⁺. Such values may indicate influence from non-sea salt sources of Cl⁻
739, such as biomass burning (Jing et al., 2017; Park et al., 2013; Cao et al., 2016), mineral dust
740 (Sullivan et al., 2007), and waste incineration (Moffet et al., 2008). Especially in December-
741 February and March, negative mass concentrations of lost Cl⁻ often occur in samples with
742 relatively high mass concentrations of bulk Ca²⁺ (Fig. S10) and K⁺ (Fig. S11), which can be
743 considered tracers for many of the non-sea salt sources of Cl⁻ mentioned above. However, there
744 are several exceptions to these relationships, and we leave a more thorough investigation into non-
745 sea salt sources of particulate Cl⁻ to future studies.



746

747 **Figure 5.** Same as Fig. 2, except for lost Cl.



748 **3.6 Attributing lost Cl⁻ to acidic species**

749 Median mass concentrations of excess acidic species have the potential to displace 0.17, 0.34,
750 0.21, 0.04, 0.26, and 1.14 $\mu\text{g m}^{-3}$ (117, 228, 141, 27, 172, and 758 pptv, respectively) of Cl⁻ from
751 sea salt particles for December-February, March, March transit, May, May transit, and June
752 Bermuda, respectively. These hypothetical losses exceed actual mass concentrations of lost Cl⁻ for
753 all categories except May and May transit, suggesting measured excess acidic species often did
754 not react to their full potential with available particulate Cl⁻, considering median %Cl⁻ depletion
755 values are 6, 10, 9, and 64% for December-February, March, March transit, and June Bermuda,
756 respectively. The extent of depletion reactions in December-February, March, March transit, and
757 June Bermuda may have been limited by meteorological variables (e.g., temperature, RH) and/or
758 restricted access of acidic species to particulate Cl⁻ due to the size distribution and/or mixing state
759 of sea salt particles (Su et al., 2022 and references therein).

760 Most lost Cl⁻ can be attributed mostly to ExNO₃⁻ in December-February, March, March transit,
761 and May transit, which is consistent with findings from past works (e.g., Nolte et al., 2008; Yao
762 and Zhang, 2012; Zhao and Gao, 2008). Excess SO₄²⁻ and ExNO₃⁻ have the potential to contribute
763 equally to Cl⁻ losses for June Bermuda, yet since actual lost Cl⁻ was much lower than theoretical
764 lost Cl⁻, the extent to which each species contributed is unknown. Oxalate has the potential to
765 displace the least Cl⁻ for all categories (0.01, 0.01, 0.01, 0.03, 0.03, and 0.02 $\mu\text{g m}^{-3}$ for December-
766 February, March, March transit, May, May transit, and June Bermuda, respectively), although it
767 is but one organic acid among thousands (Robinson et al., 2007). As mentioned above, there is
768 convincing evidence that organic acids had considerable presence in sampled air masses,
769 especially for Mar transit, May transit and May. This may be due to rising amounts of incident
770 solar radiation accelerating photochemical oxidation of abundant biogenic and anthropogenic
771 VOCs along the USEC to produce secondary organic aerosols (SOA), followed by further
772 oxidation of these SOA to produce oxygenated organics, many of which can serve as weak acids
773 in Cl⁻ depletion reactions. It is possible that unmeasured organic acids are responsible for the lost
774 Cl⁻ that currently cannot be accounted for in May and May transit, although further research is
775 necessary to explore this idea, specifically studies quantifying mass concentrations of additional
776 organic acids in the context of Cl⁻ depletion.

777
778 **3.7 Outcomes from quantifying Cl⁻ depletion semi-unconventionally**

779 In the following subsections we examine the effects of accounting for (i) dust and (ii) dust and
780 combustion emissions as a source of Na⁺, as well as focusing our discussions on mass
781 concentrations of Cl⁻ displaced from sea salt particles instead of either %Cl⁻ depletion or Cl⁻:Na⁺
782 ratios alone. We consider these to be “semi-unconventional” approaches as a handful of studies
783 have employed at least one of these methods, but they are not commonly used in Cl⁻ depletion
784 studies (based on the 76 studies presented in Table S3 in Su et al., 2022). However, we
785 acknowledge many works neglect non-sea salt sources of Na⁺ after determining crustal
786 contributions are unlikely (e.g., Rastogi et al., 2020; Bondy et al., 2017) or avoid calculating Cl⁻
787 depletion for particles of a certain size range when anthropogenic sources seem to contribute to
788 Na⁺ and/or Cl⁻ (e.g., Feng et al., 2017; Nolte et al., 2008). This work builds on past studies to
789 provide an all-encompassing method for quantifying Cl⁻ depletion in air masses influenced by dust
790 and/or combustion emissions, as well as relating Cl⁻ losses to their potential effects on atmospheric
791 oxidation processes. We now discuss when, if ever, these methods are of importance for the NWA
792 and provide a few lessons learned for future works interested in using these methods.

793



794 3.7.1 Significance of accounting for Na⁺ in dust

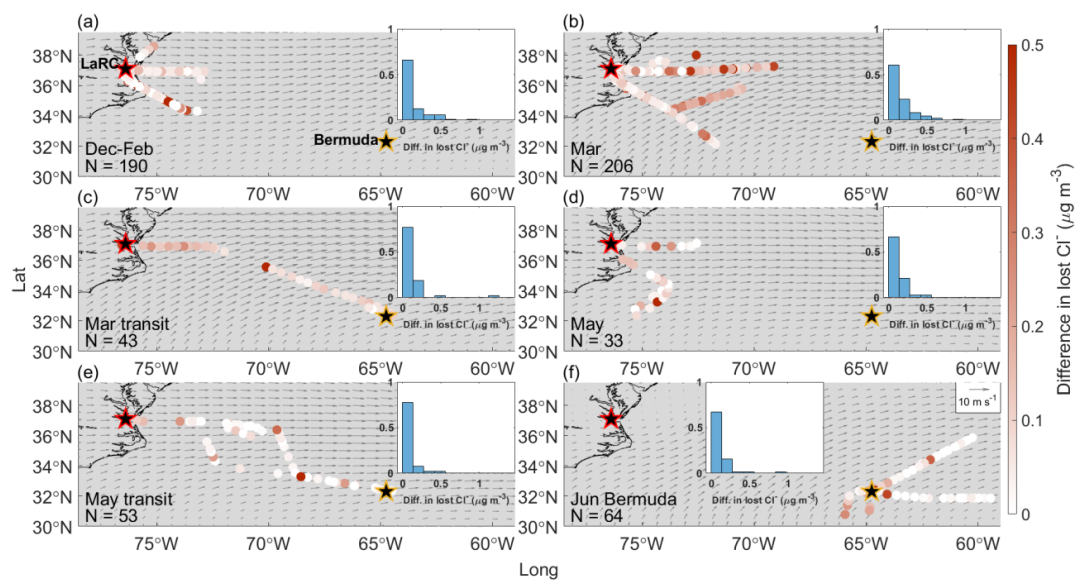
795 To facilitate understanding of the results below, recall mass concentrations of lost Cl_{diff}⁻
796 quantify the difference in estimating Cl⁻ depletion when dust is considered as a source of Na⁺
797 (Approach 1) versus when Na⁺ is attributed entirely to sea salt (Approach 2). Median lost Cl_{diff}⁻
798 mass concentrations are 0.05, 0.1, 0.09, 0.05, 0.02, and 0.01 μg m⁻³ (33, 64, 59, 34, 11, and 7 pptv,
799 respectively) for December-February, March, March transit, May, May transit, and June Bermuda,
800 respectively, meaning that Cl⁻ losses are overestimated by a factor of 2.24, 3.38, 1.80, 1.03, 1.01,
801 and 1.01, respectively, when using Approach 2 versus Approach 1. However, even though
802 overestimates are proportionately large for December-February, March, and March transit, it may
803 not be critical to account for dust as a source of Na⁺ on a seasonal scale (Fig. 6). Specifically,
804 lost Cl_{bulk}⁻ mass concentrations for December-February, March, and March transit (58, 91, and
805 133 pptv, respectively) are still well below the point where they would significantly accelerate
806 VOC oxidation in the boundary layer. Similarly, Approaches 1 and 2 both lead to the conclusion
807 that depletion reactions in May have the potential to accelerate tropospheric VOC oxidation, while
808 lost Cl_{diff}⁻ values are too small for May transit and June Bermuda to affect overarching conclusions
809 regarding relationships between Cl⁻ depletion and VOC oxidation rates. However, this study
810 reports mass concentrations of lost Cl⁻ and lost Cl_{diff}⁻ for particles with ambient diameters < 5 μm,
811 so it is possible that contributions of Na⁺ from dust particles > 5 μm may be sufficiently high to
812 lead to critical overestimates in Cl⁻ depletion, especially considering that lost Cl⁻ mass
813 concentrations may increase when additionally accounting for depletion in larger sea salt particles.

814 Although not critically important on a seasonal scale, Approaches 1 and 2 produce
815 considerably different estimates of lost Cl⁻ for several flights sampling air masses more heavily
816 influenced by dust. Median bulk Ca²⁺ mass concentrations are 5.2 and 8.2 times higher on 30
817 November and 01 December 2021 (RFs 94 and 95, respectively) than the December-February
818 median without corresponding enhancements in bulk Na⁺, suggesting a higher presence of dust
819 than usual. Using Approach 1, 100% and 88% (0.14 and 0.23 μg m⁻³, respectively) of median bulk
820 Na⁺ mass concentrations are attributed to dust for 30 November and 01 December (Table S7),
821 respectively, which results in corrections of lost Cl⁻ up to 0.63 μg m⁻³ (420 pptv) compared to
822 overestimates based on Approach 2 (Fig. 7). Dust particles sampled on these flights were likely
823 lofted in smoke plumes extending over the NWA from fires in the eastern and southeastern U.S.
824 On 03 March 2022 (RFS 131 and 132), median bulk Ca²⁺ and Na⁺ mass concentrations are 2.1 and
825 3.4 times higher, respectively, than categorical medians, as it appears the NWA was heavily
826 influenced by BB emissions from agricultural fires throughout the eastern U.S. Although only 15%
827 of the median bulk Na⁺ mass concentration is attributed to dust, lost Cl_{diff}⁻ mass concentrations are
828 as high as 1.05 μg m⁻³ (700 pptv), with most between 0.11 and 0.32 μg m⁻³ (73 - 213 pptv). As
829 mentioned in Sect. 3.3, there is interest in exploring the spatial gradient in bulk Ca²⁺ along March
830 transit flights (RFs 142 and 143) to see how estimates of Cl⁻ depletion are affected by the transition
831 from a potentially dust-influenced air mass (directly east of LaRC) to one with less dust influence
832 (to the southeast towards Bermuda). Although lost Cl_{diff}⁻ mass concentrations are lower compared
833 to those of previous case studies, Approach 2 overestimates Cl⁻ depletion more for the air mass
834 closest to the USEC compared to that closest to Bermuda. The air mass with higher bulk Ca²⁺ mass
835 concentrations appears to be composed of emissions from widespread springtime BB, and the
836 shape of the plume is such over the NWA that the aircraft would fly in it near the USEC but not
837 necessarily near Bermuda. The case studies above suggest that Cl⁻ depletion can be considerably
838 overestimated in smoke plumes when using Approach 2 as entrained dust particles can contribute
839 meaningfully to bulk Na⁺ mass concentrations, and that these overestimates may be of



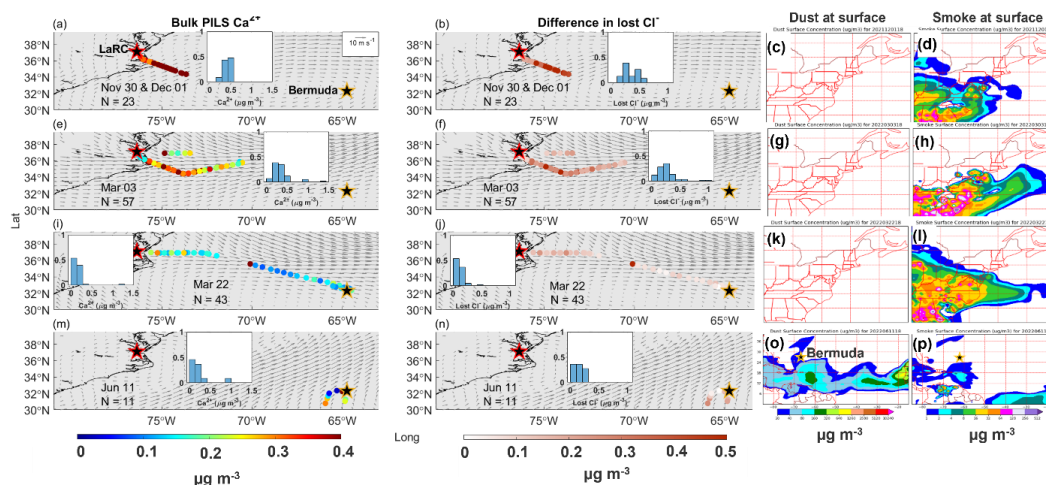
840 consequence when relating Cl^- depletion to potential increases in VOC oxidation over the region.
841 Median Ca^{2+} mass concentrations are 3 times higher ($0.21 \mu\text{g m}^{-3}$) than the June Bermuda median
842 on 11 June 2022 (RFs 172 and 173) without similar enhancements in bulk Na^+ , suggesting
843 increases in bulk Ca^{2+} are likely due to African dust sampling (as opposed to increased sea salt
844 mass concentrations). The arrival of African dust near Bermuda results in overestimates of lost Cl^-
845 up to $0.315 \mu\text{g m}^{-3}$ (210 pptv) via Approach 2, which are not large enough to affect predictions for
846 potential increases in rates of tropospheric VOC oxidation. Sampling ended near the beginning of
847 the peak season for long-range transport of African dust to the NWA (e.g., Prospero, 1996;
848 Zuidema et al., 2019), so we do not have many flights to choose from for studying effects of
849 African dust plumes on Cl^- depletion calculations. Using 6300 ppm as a mass ratio of Na^+ in dust
850 particles (Seinfeld and Pandis, 2016), 131.54 and $73.66 \mu\text{g m}^{-3}$ of dust would be necessary to cause
851 critical overestimates of lost Cl^- (i.e., lost $\text{Cl}^-_{\text{bulk}}$ values would reach $1.5 \mu\text{g m}^{-3}$ using Approach 2)
852 assuming 0 and $0.66 \mu\text{g m}^{-3}$ of Cl^- were already being displaced from sea salt particles, respectively
853 (note $0.66 \mu\text{g m}^{-3}$ is the median lost Cl^- value for June Bermuda). Edwards et al. (2021) reported
854 peak African dust mass concentrations of $73.32 \mu\text{g m}^{-3}$ near Miami, Florida, so it may be possible
855 for values to reach these levels over Bermuda, but it would take a relatively large plume. Therefore,
856 it is typically not critical to use Approach 1 when quantifying Cl^- depletion near Bermuda, yet it
857 may be important to use this approach during strong African dust events.

858 Furthermore, past works have demonstrated the uptake of precursors to acidic species (e.g.,
859 NO_x , SO_2 ; Grassian, 2002; Hanisch and Crowley, 2003; Ullerstam et al., 2002), inorganic acids
860 (e.g., H_2SO_4 , HNO_3 ; Ooki and Uematsu, 2005; Sullivan et al., 2007), organic acids (Al-Hosney et
861 al., 2005; Carlos-Cuellar et al., 2003), and HCl (Zhang and Iwasaka, 2001; Ooki and Uematsu,
862 2005; Sullivan et al., 2007; Santschi and Rossi, 2006; Sorooshian et al., 2012) on dust particles.
863 Thus, in addition to considering dust as a source of Na^+ , it may also be important to account for its
864 presence to avoid overestimating Cl^- depletion and its impacts on atmospheric oxidation as (i)
865 uptake of acidic species and their precursors may reduce amounts available for depletion reactions,
866 and (ii) deposition of HCl on dust particles may reduce the amount of Cl radicals produced
867 following Cl^- displacement.



868

869 **Figure 6.** Same as Fig. 2, except for differences in lost Cl^- when sea salt is assumed to be the only
870 source of bulk Na^+ versus when sea salt and dust are both considered to contribute to bulk Na^+
871 mass concentrations.



872

873 **Figure 7.** Spatial relationships between mass concentrations of (a) bulk PILS Ca^{2+} and (b)
874 differences in lost Cl^- , as well as NAAPS reanalysis surface mass concentrations of (c) dust and
875 smoke for the case study on 30 November – 01 December 2022 (RFs 94 and 95). The second,
876 third, and fourth rows correspond to case studies on 03 March (RFs 131 and 132), 22 March (RFs
877 142 and 143), and 11 June (RFs 172 and 173) 2022, respectively, where (e, f, g, h), (i, j, k, l), and
878 (m, n, o, p) display the same variables as (a, b, c, d), respectively. Normalized histograms for bulk
879 PILS Ca^{2+} and differences in lost Cl^- show the distribution of values for that specific case study
880 since overlap among the colored dots can hide some from view. Grey arrows indicate the average
881 magnitude and direction of MERRA-2 winds at 950 hPa for the month(s) relevant to each category.
882 NASA Langley Research Center (LaRC) and Bermuda are marked with red-edged and golden-
883 edged stars, respectively.



884 **3.7.2 Significance of accounting for Na⁺ in dust and combustion-sourced particles**

885 As shown above, air masses influenced by BB frequently advect over the NWA, especially in
886 March, occasionally increasing dust mass concentrations to levels capable of causing considerable
887 overestimates in Cl⁻ depletion. However, there is little to no effect on Cl⁻ depletion calculations
888 when accounting for contributions to Na⁺ from combustion particles emitted via agricultural
889 burning and forest fires as median Na_{comb}⁺ mass concentrations are 0.00 μg m⁻³ for all categories
890 (Tables S8 and S9, respectively). Therefore, it may be more important to quantify contributions of
891 dust as opposed to the combustion-sourced particles in smoke plumes over the NWA to avoid
892 overestimates of Cl⁻ depletion. However, recall median bulk K⁺ mass concentrations for this study
893 are 2 and 14 times lower than values measured in air masses more heavily influenced by (i)
894 agricultural burning (Kacenenbogen et al., 2022) and (ii) wildfire smoke (Adachi et al., 2022),
895 respectively. Thus, it is possible quantifying Na_{comb}⁺ is important for accurate estimates of Cl⁻
896 depletion in more concentrated BB plumes, yet we cannot explore this with the flights available
897 and leave such an investigation to future studies. When combustion emissions are attributed to
898 industrial operations, residential wood burning in sauna stoves, car driving, or coal burning at
899 power plants, there is also no influence on Cl⁻ depletion calculations for any category (i.e., all
900 median Na_{comb}⁺ values are 0.00 μg m⁻³; Tables S10 – S13). Thus, particles generated by the myriad
901 of combustion processes occurring along the eastern U.S. may be too dilute over the NWA to affect
902 calculations of Cl⁻ depletion not only in air masses reaching Bermuda but also in those much closer
903 to the USEC (e.g., Fig. S12).

904 Since mass concentrations of Na_{comb}⁺ are typically negligible, Eqs. 1 – 4 and 6 – 13 should
905 provide the same median mass concentrations of ssNa⁺ and Na_{dust}⁺ for each category. However,
906 many samples are excluded when using Eqs. 6 – 13 as their K⁺ mass concentrations are below IC
907 detection limits, causing adjustments in median ssNa⁺ and Na_{dust}⁺ values for several categories.
908 Despite the advantages in accounting for non-sea salt sources of Na⁺, one disadvantage is potential
909 dataset reduction. For example, 275, 246, 48, 113, 106, and 81 samples provide bulk Na⁺ mass
910 concentrations for December-February, March, March transit, May, May transit, and June
911 Bermuda, respectively, yet only 202, 220, 48, 64, 75, and 66, respectively, can be used in Eqs. 1 –
912 4, with even fewer available for use in Eqs. 6 – 13 where concurrent mass concentrations of bulk
913 Na⁺, Ca²⁺, and K⁺ are necessary. Thus, future studies may want to weigh the consequences of
914 neglecting contributions of Na⁺ from non-sea salt sources versus potential reductions to the number
915 of samples included in statistical analyses.

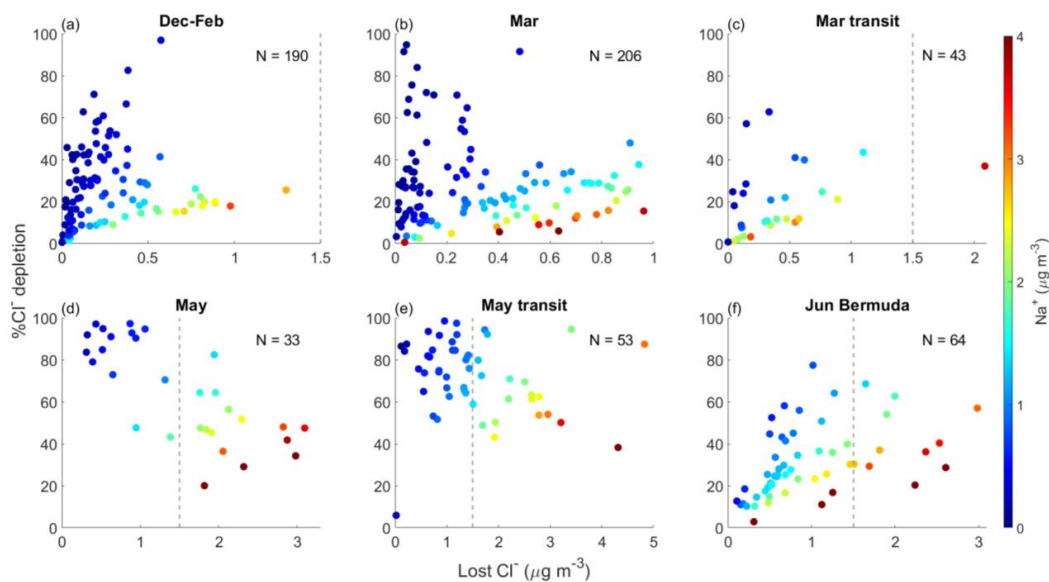
916

917 **3.7.3 Significance of focusing on lost Cl⁻ instead of %Cl⁻ depletion**

918 Values of %Cl⁻ depletion display similar trends to lost Cl⁻ mass concentrations, where most
919 percentages are (i) relatively low for December-February, March, and March transit (half are ≤
920 10%, nearly all are ≤ 50%), (ii) relatively high for May and May transit (nearly all are > 40%),
921 and (iii) relatively moderate for June Bermuda (values are distributed fairly evenly from 0 – 30%,
922 and nearly all are ≤ 60%, Fig. S13). However, these %Cl⁻ depletion values can only be used to
923 show relative seasonal/categorical differences, and they cannot (i) inform when Cl⁻ mass transfer
924 is greatest from the particulate to gas phase or (ii) place such depletion reactions in the context of
925 their potential influence on tropospheric VOC oxidation rates. For example, samples with higher
926 %Cl⁻ depletion values can easily be misinterpreted as having greater Cl⁻ losses when in reality the



927 opposite may be true. Lost Cl^- and $\% \text{Cl}^-$ depletion have a negative correlation for May and May
928 transit, meaning that samples with the least (most) displaced Cl^- have the highest (lowest) $\% \text{Cl}^-$
929 depletion values (Fig. 8). The remaining categories have mostly positive correlations between lost
930 Cl^- and $\% \text{Cl}^-$ depletion, although $\% \text{Cl}^-$ depletion values are typically higher for samples with
931 relatively low bulk Na^+ mass concentrations at a fixed lost Cl^- value. This trend may be due to
932 samples containing sea salt particles with varying size distributions (i.e., lower bulk Na^+ mass
933 concentrations may mean smaller sea salt particles were collected in a given sample) and
934 considering that smaller sea salt particles are typically more susceptible to depletion reactions (e.g.,
935 Su et al., 2022 and references therein). However, this behavior may also be an artifact of increased
936 sensitivity of $\% \text{Cl}^-$ depletion to samples with relatively small ssNa^+ mass concentrations. Many of
937 the samples with mass concentrations of lost Cl^- high enough to potentially influence VOC
938 oxidation rates (i.e., lost $\text{Cl}^- > 1.5 \mu\text{g m}^{-3}$) have $\% \text{Cl}^-$ depletion values $< 40\%$, while nearly all
939 samples with $\% \text{Cl}^-$ depletion values $> 80\%$ do not have Cl^- losses capable of affecting such rates.
940 Thus, we highly recommend future studies quantify mass concentrations of lost Cl^- to make results
941 from depletion studies more suitable for understanding mass exchange between sea salt particles
942 and the surrounding atmosphere and the consequences this can have on rates of tropospheric
943 chemistry and radiative forcing.



944

945 **Figure 8.** Relationships between mass concentrations of lost Cl^- and $\% \text{Cl}^-$ depletion for (a)
946 December-February, (b) March, (c) March transit, (d) May, (e) May transit, and (f) June Bermuda.
947 Markers are colored by bulk PILS Na^+ mass concentrations, and the vertical dashed gray line in
948 some panels denotes where mass concentrations of lost Cl^- may begin to have considerable
949 influence on tropospheric VOC oxidation rates.



950 4. Conclusions

951 This study investigates Cl^- depletion in sea salt particles over the NWA from approximately
952 December 2021 – June 2022 using an airborne dataset quantifying the chemical composition of
953 particles $< 5 \mu\text{m}$ among other parameters throughout the lower 3 km of the atmosphere. Trends in
954 bulk PILS Na^+ suggest sea salt mass concentrations (1) do not exhibit seasonal variation but are
955 reduced following the passage of MLCs near the USEC, and (2) are higher in the open-ocean
956 environment of Bermuda than along the USEC. Losses of Cl^- are greatest in May and least in
957 December-February and March, with median lost Cl^- mass concentrations of 1.76, 0.04, and 0.04
958 $\mu\text{g m}^{-3}$ (1174, 27, and 27 pptv), respectively. Mass concentrations of measured excess acidic
959 species can account for all the Cl^- depletion observed in December-February, March, and June
960 near Bermuda, yet none in May, suggesting unmeasured organic acids may be largely responsible
961 for displacement in certain months. Accounting for dust as a source of Na^+ is not critical for
962 accurately predicting how Cl^- depletion reactions will influence rates of tropospheric VOC
963 oxidation on a seasonal basis, yet this may be important for large smoke and dust plumes over the
964 NWA. Combustion-sourced particles do not contribute enough Na^+ to meaningfully affect Cl^-
965 depletion estimates in any season for the air masses sampled. Finally, quantifying Cl^- depletion as
966 a percentage sufficiently captures seasonal trends in depletion processes but fails to convey the
967 effects they may have on atmospheric oxidation rates.

968 These results help address several uncertainties regarding Cl^- depletion over the NWA and its
969 influence on regional oxidation cycles. First, by identifying factors affecting regional sea salt mass
970 concentrations, we help advance the scientific community towards better understanding and
971 forecasting of regional fluctuations in this major reactive atmospheric Cl reservoir. Additionally,
972 seasonally resolved mass concentrations of lost Cl^- reveal that depletion reactions correspond to
973 increases in reactive chlorine-containing gases capable of producing concentrations of Cl radicals
974 sufficient to oxidize 20 – 40% of nonmethane alkanes in the marine troposphere in May, which
975 can have numerous implications including potentially accelerating O_3 production over this highly
976 populated region. The possibility for dust to cause meaningful overestimates of Cl^- depletion is a
977 regionally novel finding and should encourage future studies and modeling efforts to monitor and
978 account for smoke and dust plumes advecting over the NWA when quantifying sea salt reactivity.
979 Additionally, our results reveal the importance in quantifying absolute Cl^- losses as samples with
980 the highest values of % Cl^- depletion often have relatively low Cl^- losses, and lost Cl^- and % Cl^-
981 depletion are negatively correlated in May, which is critical to recognize as Cl^- depletion has the
982 greatest potential effect on tropospheric VOC oxidation rates during this month compared to all
983 other studied.

984 Lost Cl^- mass concentrations are similar between median values reported in this study and the
985 mean presented in Keene et al. (1990) for summertime conditions around Bermuda (0.66 and 0.68
986 $\mu\text{g m}^{-3}$, respectively), while our values also fall within the range observed over Bermuda in spring
987 (0.22 – 1.35 $\mu\text{g m}^{-3}$; Keene and Savoie, 1998). Keene et al. (1990) reported lower lost Cl^- mass
988 concentrations along the USEC from July-September than our findings in May (1.11 and 1.76 $\mu\text{g m}^{-3}$
989 $\mu\text{g m}^{-3}$, respectively), while our median in May is above the range shared in Keene et al. (2007) for
990 July-August (0 – 1.31 $\mu\text{g m}^{-3}$). Haskins et al. (2018) quantified median lost Cl^- mass concentrations
991 of 0.30 $\mu\text{g m}^{-3}$ over the ocean from February – March, which is 7 times higher than our medians
992 for December-February and March (0.04 and 0.04 $\mu\text{g m}^{-3}$, respectively), yet note their study
993 specifically targeted polluted winter air masses while ours did not. Many past works along the
994 North American east coast have been able to attribute Cl^- depletion largely to inorganic acids in
995 the summer and fall (Zhao and Gao, 2008; Keene et al., 2007; Nolte et al., 2008; Yao and Zhang,



1996 2012), with Keene et al. (1990) reporting a lowest contribution of 38%. We can attribute all Cl⁻
1997 depletion to inorganic acids in December-February, March, and June, yet find inorganic acids do
1998 not contribute at all to displacement reactions in May. Our study suggests depletion reactions are
1999 still occurring to the extent they were in the 1990s and 2000s over the NWA except that organic
1000 acids are possibly becoming increasingly responsible for Cl⁻ displacement, especially in May,
1001 although further research is needed to verify this.

1002 Although the ACTIVATE dataset is well-equipped to explore seasonal and spatial trends in
1003 Cl⁻ depletion over the NWA, there are several caveats and limitations to be mindful of when
1004 reviewing our results. Reported mass concentrations of sea salt and lost Cl⁻ should be interpreted
1005 as a lower limit due to the size range of particles sampled (< 5 μm). Additionally, calculations for
1006 the neutralization of SO₄²⁻ and NO₃⁻ by NH₄⁺ combine speciated mass concentrations from two
1007 separate instruments, each considering a different size range of particles, meaning mass
1008 concentrations of excess acidic species should be considered as an upper limit for particles < 5
1009 μm. We recommend accounting for non-sea salt sources of Na⁺ when appropriate but acknowledge
1010 that it may limit statistical analyses as the procedure for disentangling contributions of various
1011 sources to bulk Na⁺ requires synchronous mass concentrations of multiple species.

1012 Overall, this study presents an updated account of sea salt reactivity over the NWA while also
1013 providing unprecedented statistics for (i) responses in parameters relevant to Cl⁻ depletion to
1014 passing frontal systems, (ii) sea salt particle mass concentrations within the lower 3 km of the
1015 atmosphere between the USEC and Bermuda, (iii) the extent of Cl⁻ depletion occurring in a variety
1016 of air masses in winter, spring, and early summer as well as the importance of (iv) accounting for
1017 smoke and dust plumes as a source of Na⁺ and (v) quantifying Cl⁻ depletion absolutely instead of
1018 relatively. Our finding that depletion reactions are extensive enough to alter rates of VOC
1019 oxidation along the USEC in May is impactful on multiple levels ranging from human health to
1020 regional radiative forcing, while reporting that inorganic acidic species are not contributing to
1021 these losses informs future works and the chemical modeling community that additional acidic
1022 species are critical to first identify and then to monitor. Finally, this study reveals the limitations
1023 in using traditional methods when quantifying Cl⁻ depletion and will hopefully motivate future
1024 works to either be mindful of these limitations or choose alternative methods.

1025 **Data availability**

1026 The ACTIVATE dataset can be found at
1027 <https://doi.org/10.5067/SUBORBITAL/ACTIVATE/DATA001> (ACTIVATE Science Team,
1028 2020). Level-3 (8-day, 4 km resolution) sea surface chlorophyll a concentrations from MODIS-
1029 Aqua can be found at <https://doi.org/10.5067/AQUA/MODIS/L3M/CHL/2022>.

1030 **Author contributions**

1031 YC, ECC, JPD, GSD, CER, MAS, ELW, and LDZ collected and/or prepared the data. ELE
1032 conducted the data analysis. ELE, ECC, and AS conducted data interpretation. ELE and AS
1033 prepared the manuscript with editing from ECC, JPD, GSD, MAS, ELW, and LDZ.



1034 **Competing interests**

1035 At least one of the (co-)authors is a member of the editorial board of Atmospheric Chemistry and
1036 Physics.

1037 **Disclaimer**

1038 Publisher's note: Copernicus Publications remains neutral with regard to jurisdictional claims in
1039 published maps and institutional affiliations.

1040

1041 **Acknowledgements**

1042 The authors acknowledge Claire Robinson for her contributions to this study and dedicate this to
1043 her. We thank pilots and aircraft maintenance personnel of NASA Langley Research Services
1044 Directorate for successfully conducting ACTIVATE flights and all others who were involved in
1045 executing the ACTIVATE campaign.

1046 **Financial support**

1047 This work was funded by ACTIVATE, a NASA Earth Venture Suborbital-3 (EVS-3) investigation
1048 funded by NASA's Earth Science Division and managed through the Earth System Science
1049 Pathfinder Program Office. University of Arizona investigators were funded by NASA grant no.
1050 80NSSC19K0442 and ONR grant no. N00014-21-1-2115.



1051 **References**

1052 ACTIVATE Science Team: Aerosol Cloud meTeorology Interactions oVer the western ATlantic
1053 Experiment Data, <https://doi.org/10.5067/SUBORBITAL/ACTIVATE/DATA001>, 2020.

1054 Adachi, K., Dibb, J. E., Scheuer, E., Katich, J. M., Schwarz, J. P., Perring, A. E., Mediavilla, B.,
1055 Guo, H., Campuzano-Jost, P., Jimenez, J. L., Crawford, J., Soja, A. J., Oshima, N., Kajino, M.,
1056 Kinase, T., Kleinman, L., Sedlacek III, A. J., Yokelson, R. J., and Buseck, P. R.: Fine Ash-
1057 Bearing Particles as a Major Aerosol Component in Biomass Burning Smoke, *Journal of*
1058 *Geophysical Research: Atmospheres*, 127, e2021JD035657,
1059 <https://doi.org/10.1029/2021JD035657>, 2022.

1060 Akagi, S. K., Yokelson, R. J., Burling, I. R., Meinardi, S., Simpson, I., Blake, D. R.,
1061 McMeeking, G. R., Sullivan, A., Lee, T., Kreidenweis, S., Urbanski, S., Reardon, J., Griffith, D.
1062 W. T., Johnson, T. J., and Weise, D. R.: Measurements of reactive trace gases and variable O₃
1063 formation rates in some South Carolina biomass burning plumes, *Atmospheric Chemistry and*
1064 *Physics*, 13, 1141–1165, <https://doi.org/10.5194/acp-13-1141-2013>, 2013.

1065 Aldhaif, A. M., Lopez, D. H., Dadashazar, H., and Sorooshian, A.: Sources, frequency, and
1066 chemical nature of dust events impacting the United States East Coast, *Atmospheric*
1067 *Environment*, 231, 117456, <https://doi.org/10.1016/j.atmosenv.2020.117456>, 2020.

1068 Al-Hosney, H. A., Carlos-Cuellar, S., Baltrusaitis, J., and Grassian, V. H.: Heterogeneous uptake
1069 and reactivity of formic acid on calcium carbonate particles: a Knudsen cell reactor, FTIR and
1070 SEM study, *Phys. Chem. Chem. Phys.*, 7, 3587–3595, <https://doi.org/10.1039/B510112C>, 2005.

1071 Andreae, M. O. and Merlet, P.: Emission of trace gases and aerosols from biomass burning,
1072 *Global Biogeochemical Cycles*, 15, 955–966, <https://doi.org/10.1029/2000GB001382>, 2001.

1073 Andreae, M. O., Andreae, T. W., Annegarn, H., Beer, J., Cachier, H., Le Canut, P., Elbert, W.,
1074 Maenhaut, W., Salma, I., Wienhold, F. G., and Zenker, T.: Airborne studies of aerosol emissions
1075 from savanna fires in southern Africa: 2. Aerosol chemical composition, *Journal of Geophysical*
1076 *Research: Atmospheres*, 103, 32119–32128, <https://doi.org/10.1029/98JD02280>, 1998.

1077 Andreae, M. O., Andreae, T. W., Meyerdierks, D., and Thiel, C.: Marine sulfur cycling and the
1078 atmospheric aerosol over the springtime North Atlantic, *Chemosphere*, 52, 1321–1343,
1079 [https://doi.org/10.1016/S0045-6535\(03\)00366-7](https://doi.org/10.1016/S0045-6535(03)00366-7), 2003.

1080 AzadiAghdam, M., Braun, R. A., Edwards, E.-L., Bañaga, P. A., Cruz, M. T., Betito, G.,
1081 Cambaliza, M. O., Dadashazar, H., Lorenzo, G. R., Ma, L., MacDonald, A. B., Nguyen, P.,
1082 Simpas, J. B., Stahl, C., and Sorooshian, A.: On the nature of sea salt aerosol at a coastal
1083 megacity: Insights from Manila, Philippines in Southeast Asia, *Atmospheric Environment*, 216,
1084 116922, <https://doi.org/10.1016/j.atmosenv.2019.116922>, 2019.

1085 Bondy, A. L., Wang, B., Laskin, A., Craig, R. L., Nhliziyo, M. V., Bertman, S. B., Pratt, K. A.,
1086 Shepson, P. B., and Ault, A. P.: Inland Sea Spray Aerosol Transport and Incomplete Chloride
1087 Depletion: Varying Degrees of Reactive Processing Observed during SOAS, *Environ. Sci.*
1088 *Technol.*, 51, 9533–9542, <https://doi.org/10.1021/acs.est.7b02085>, 2017.



- 1089 Boreddy, S. K. R. and Kawamura, K.: A 12-year observation of water-soluble ions in TSP
1090 aerosols collected at a remote marine location in the western North Pacific: an outflow region of
1091 Asian dust, *Atmospheric Chemistry and Physics*, 15, 6437–6453, [https://doi.org/10.5194/acp-15-](https://doi.org/10.5194/acp-15-6437-2015)
1092 6437-2015, 2015.
- 1093 Bowen, H. J. M.: *Environmental chemistry of the elements*, Academic Press, London, New
1094 York, xv, 333 pp., 1979.
- 1095 Braun, R. A., Dadashazar, H., MacDonald, A. B., Aldhaif, A. M., Maudlin, L. C., Crosbie, E.,
1096 Aghdam, M. A., Hossein Mardi, A., and Sorooshian, A.: Impact of Wildfire Emissions on
1097 Chloride and Bromide Depletion in Marine Aerosol Particles, *Environ. Sci. Technol.*, 51, 9013–
1098 9021, <https://doi.org/10.1021/acs.est.7b02039>, 2017.
- 1099 Braun, R. A., McComiskey, A., Tselioudis, G., Tropf, D., and Sorooshian, A.: Cloud, Aerosol,
1100 and Radiative Properties Over the Western North Atlantic Ocean, *Journal of Geophysical*
1101 *Research: Atmospheres*, 126, e2020JD034113, <https://doi.org/10.1029/2020JD034113>, 2021.
- 1102 Buchholz, R. R., Worden, H. M., Park, M., Francis, G., Deeter, M. N., Edwards, D. P., Emmons,
1103 L. K., Gaubert, B., Gille, J., Martínez-Alonso, S., Tang, W., Kumar, R., Drummond, J. R.,
1104 Clerbaux, C., George, M., Coheur, P.-F., Hurtmans, D., Bowman, K. W., Luo, M., Payne, V. H.,
1105 Worden, J. R., Chin, M., Levy, R. C., Warner, J., Wei, Z., and Kulawik, S. S.: Air pollution
1106 trends measured from Terra: CO and AOD over industrial, fire-prone, and background regions,
1107 *Remote Sensing of Environment*, 256, 112275, <https://doi.org/10.1016/j.rse.2020.112275>, 2021.
- 1108 Cao, F., Zhang, S.-C., Kawamura, K., and Zhang, Y.-L.: Inorganic markers, carbonaceous
1109 components and stable carbon isotope from biomass burning aerosols in Northeast China,
1110 *Science of The Total Environment*, 572, 1244–1251,
1111 <https://doi.org/10.1016/j.scitotenv.2015.09.099>, 2016.
- 1112 Carlos-Cuellar, S., Li, P., Christensen, A. P., Krueger, B. J., Burrichter, C., and Grassian, V. H.:
1113 Heterogeneous Uptake Kinetics of Volatile Organic Compounds on Oxide Surfaces Using a
1114 Knudsen Cell Reactor: Adsorption of Acetic Acid, Formaldehyde, and Methanol on α -Fe₂O₃, α -
1115 Al₂O₃, and SiO₂, *J. Phys. Chem. A*, 107, 4250–4261, <https://doi.org/10.1021/jp0267609>, 2003.
- 1116 Chameides, W. L. and Stelson, A. W.: Reply [to “Comment on ‘Aqueous phase chemical
1117 processes in deliquescent sea-salt aerosols: A mechanism that couples the atmospheric cycles of
1118 S and sea salt’ by W. L. Chameides and A. W. Stelson”], *Journal of Geophysical Research:*
1119 *Atmospheres*, 98, 9051–9054, <https://doi.org/10.1029/93JD00310>, 1993.
- 1120 Chatterjee, A., Dutta, M., Ghosh, A., Ghosh, S. K., and Roy, A.: Relative role of black carbon
1121 and sea-salt aerosols as cloud condensation nuclei over a high altitude urban atmosphere in
1122 eastern Himalaya, *Science of The Total Environment*, 742, 140468,
1123 <https://doi.org/10.1016/j.scitotenv.2020.140468>, 2020.
- 1124 Chen, Z., Liu, P., Liu, Y., and Zhang, Y.-H.: Strong Acids or Bases Displaced by Weak Acids or
1125 Bases in Aerosols: Reactions Driven by the Continuous Partitioning of Volatile Products into the
1126 Gas Phase, *Acc. Chem. Res.*, 54, 3667–3678, <https://doi.org/10.1021/acs.accounts.1c00318>,
1127 2021.



- 1128 Cooper, O. R., Moody, J. L., Parrish, D. D., Trainer, M., Ryerson, T. B., Holloway, J. S., Hübler,
1129 G., Fehsenfeld, F. C., Oltmans, S. J., and Evans, M. J.: Trace gas signatures of the airstreams
1130 within North Atlantic cyclones: Case studies from the North Atlantic Regional Experiment
1131 (NARE '97) aircraft intensive, *Journal of Geophysical Research: Atmospheres*, 106, 5437–5456,
1132 <https://doi.org/10.1029/2000JD900574>, 2001.
- 1133 Cooper, O. R., Moody, J. L., Parrish, D. D., Trainer, M., Holloway, J. S., Hübler, G., Fehsenfeld,
1134 F. C., and Stohl, A.: Trace gas composition of midlatitude cyclones over the western North
1135 Atlantic Ocean: A seasonal comparison of O₃ and CO, *Journal of Geophysical Research:*
1136 *Atmospheres*, 107, ACH 2-1-ACH 2-12, <https://doi.org/10.1029/2001JD000902>, 2002.
- 1137 Corral, A. F., Braun, R. A., Cairns, B., Gorrooh, V. A., Liu, H., Ma, L., Mardi, A. H., Painemal,
1138 D., Stannnes, S., van Dierenhoven, B., Wang, H., Yang, Y., Zhang, B., and Sorooshian, A.: An
1139 Overview of Atmospheric Features Over the Western North Atlantic Ocean and North American
1140 East Coast – Part 1: Analysis of Aerosols, Gases, and Wet Deposition Chemistry, *Journal of*
1141 *Geophysical Research: Atmospheres*, 126, e2020JD032592,
1142 <https://doi.org/10.1029/2020JD032592>, 2021.
- 1143 Corral, A. F., Choi, Y., Collister, B. L., Crosbie, E., Dadashazar, H., DiGangi, J. P., Diskin, G.
1144 S., Fenn, M., Kirschler, S., Moore, R. H., Nowak, J. B., Shook, M. A., Stahl, C. T., Shingler, T.,
1145 Thornhill, K. L., Voigt, C., Ziemba, L. D., and Sorooshian, A.: Dimethylamine in cloud water: a
1146 case study over the northwest Atlantic Ocean, *Environ. Sci.: Atmos.*, 2, 1534–1550,
1147 <https://doi.org/10.1039/D2EA00117A>, 2022.
- 1148 Crosbie, E., Shook, M. A., Ziemba, L. D., Anderson, B. E., Braun, R. A., Brown, M. D., Jordan,
1149 C. E., MacDonald, A. B., Moore, R. H., Nowak, J. B., Robinson, C. E., Shingler, T., Sorooshian,
1150 A., Stahl, C., Thornhill, K. L., Wiggins, E. B., and Winstead, E.: Coupling an online ion
1151 conductivity measurement with the particle-into-liquid sampler: Evaluation and modeling using
1152 laboratory and field aerosol data, *Aerosol Science and Technology*, 54, 1542–1555,
1153 <https://doi.org/10.1080/02786826.2020.1795499>, 2020.
- 1154 Crosbie, E., Ziemba, L. D., Shook, M. A., Robinson, C. E., Winstead, E. L., Thornhill, K. L.,
1155 Braun, R. A., MacDonald, A. B., Stahl, C., Sorooshian, A., van den Heever, S. C., DiGangi, J.
1156 P., Diskin, G. S., Woods, S., Bañaga, P., Brown, M. D., Gallo, F., Hilario, M. R. A., Jordan, C.
1157 E., Leung, G. R., Moore, R. H., Sanchez, K. J., Shingler, T. J., and Wiggins, E. B.: Measurement
1158 report: Closure analysis of aerosol–cloud composition in tropical maritime warm convection,
1159 *Atmospheric Chemistry and Physics*, 22, 13269–13302, [https://doi.org/10.5194/acp-22-13269-](https://doi.org/10.5194/acp-22-13269-2022)
1160 2022, 2022.
- 1161 Cruz, M. T., Bañaga, P. A., Betito, G., Braun, R. A., Stahl, C., Aghdam, M. A., Cambaliza, M.
1162 O., Dadashazar, H., Hilario, M. R., Lorenzo, G. R., Ma, L., MacDonald, A. B., Pabroa, P. C.,
1163 Yee, J. R., Simpas, J. B., and Sorooshian, A.: Size-resolved composition and morphology of
1164 particulate matter during the southwest monsoon in Metro Manila, Philippines, *Atmospheric*
1165 *Chemistry and Physics*, 19, 10675–10696, <https://doi.org/10.5194/acp-19-10675-2019>, 2019.
- 1166 Dadashazar, H., Alipanah, M., Hilario, M. R. A., Crosbie, E., Kirschler, S., Liu, H., Moore, R.
1167 H., Peters, A. J., Scarino, A. J., Shook, M., Thornhill, K. L., Voigt, C., Wang, H., Winstead, E.,



- 1168 Zhang, B., Ziemba, L., and Sorooshian, A.: Aerosol responses to precipitation along North
1169 American air trajectories arriving at Bermuda, *Atmospheric Chemistry and Physics*, 21, 16121–
1170 16141, <https://doi.org/10.5194/acp-21-16121-2021>, 2021.
- 1171 Dang, C., Segal-Rozenhaimer, M., Che, H., Zhang, L., Formenti, P., Taylor, J., Dobracki, A.,
1172 Purdue, S., Wong, P.-S., Nenes, A., Sedlacek III, A., Coe, H., Redemann, J., Zuidema, P.,
1173 Howell, S., and Haywood, J.: Biomass burning and marine aerosol processing over the southeast
1174 Atlantic Ocean: a TEM single-particle analysis, *Atmospheric Chemistry and Physics*, 22, 9389–
1175 9412, <https://doi.org/10.5194/acp-22-9389-2022>, 2022.
- 1176 Davis, R. E., Hayden, B. P., Gay, D. A., Phillips, W. L., and Jones, G. V.: The North Atlantic
1177 Subtropical Anticyclone, *Journal of Climate*, 10, 728–744, [https://doi.org/10.1175/1520-0442\(1997\)010<0728:TNASA>2.0.CO;2](https://doi.org/10.1175/1520-0442(1997)010<0728:TNASA>2.0.CO;2), 1997.
- 1179 DeCarlo, P. F., Dunlea, E. J., Kimmel, J. R., Aiken, A. C., Sueper, D., Crouse, J., Wennberg, P.
1180 O., Emmons, L., Shinozuka, Y., Clarke, A., Zhou, J., Tomlinson, J., Collins, D. R., Knapp, D.,
1181 Weinheimer, A. J., Montzka, D. D., Campos, T., and Jimenez, J. L.: Fast airborne aerosol size
1182 and chemistry measurements above Mexico City and Central Mexico during the MILAGRO
1183 campaign, *Atmospheric Chemistry and Physics*, 8, 4027–4048, <https://doi.org/10.5194/acp-8-4027-2008>, 2008.
- 1185 DiGangi, J. P., Choi, Y., Nowak, J. B., Halliday, H. S., Diskin, G. S., Feng, S., Barkley, Z. R.,
1186 Lauvaux, T., Pal, S., Davis, K. J., Baier, B. C., and Sweeney, C.: Seasonal Variability in Local
1187 Carbon Dioxide Biomass Burning Sources Over Central and Eastern US Using Airborne In Situ
1188 Enhancement Ratios, *Journal of Geophysical Research: Atmospheres*, 126, e2020JD034525,
1189 <https://doi.org/10.1029/2020JD034525>, 2021.
- 1190 Diskin, G. S., Podolske, J. R., Sachse, G. W., and Slate, T. A.: Open-path airborne tunable diode
1191 laser hygrometer, in: *Diode Lasers and Applications in Atmospheric Sensing, Diode Lasers and
1192 Applications in Atmospheric Sensing*, 196–204, <https://doi.org/10.1117/12.453736>, 2002.
- 1193 Drozd, G., Woo, J., Häkkinen, S. a. K., Nenes, A., and McNeill, V. F.: Inorganic salts interact
1194 with oxalic acid in submicron particles to form material with low hygroscopicity and volatility,
1195 *Atmospheric Chemistry and Physics*, 14, 5205–5215, <https://doi.org/10.5194/acp-14-5205-2014>,
1196 2014.
- 1197 Echalar, F., Gaudichet, A., Cachier, H., and Artaxo, P.: Aerosol emissions by tropical forest and
1198 savanna biomass burning: Characteristic trace elements and fluxes, *Geophysical Research
1199 Letters*, 22, 3039–3042, <https://doi.org/10.1029/95GL03170>, 1995.
- 1200 Edwards, E.-L., Corral, A. F., Dadashazar, H., Barkley, A. E., Gaston, C. J., Zuidema, P., and
1201 Sorooshian, A.: Impact of various air mass types on cloud condensation nuclei concentrations
1202 along coastal southeast Florida, *Atmospheric Environment*, 254, 118371,
1203 <https://doi.org/10.1016/j.atmosenv.2021.118371>, 2021.
- 1204 Eichler, T. and Higgins, W.: Climatology and ENSO-Related Variability of North American
1205 Extratropical Cyclone Activity, *Journal of Climate*, 19, 2076–2093,
1206 <https://doi.org/10.1175/JCLI3725.1>, 2006.



- 1207 Faxon, C. B. and Allen, D. T.: Chlorine chemistry in urban atmospheres: a review, *Environ.*
1208 *Chem.*, 10, 221–233, <https://doi.org/10.1071/EN13026>, 2013.
- 1209 Fehsenfeld, F. C., Ancellet, G., Bates, T. S., Goldstein, A. H., Hardesty, R. M., Honrath, R.,
1210 Law, K. S., Lewis, A. C., Leitch, R., McKeen, S., Meagher, J., Parrish, D. D., Pszenny, A. A.
1211 P., Russell, P. B., Schlager, H., Seinfeld, J., Talbot, R., and Zbinden, R.: International
1212 Consortium for Atmospheric Research on Transport and Transformation (ICARTT): North
1213 America to Europe—Overview of the 2004 summer field study, *Journal of Geophysical*
1214 *Research (Atmospheres)*, 111, D23S01, <https://doi.org/10.1029/2006JD007829>, 2006.
- 1215 Feng, J., Chan, E., and Vet, R.: Air quality in the eastern United States and Eastern Canada for
1216 1990–2015: 25 years of change in response to emission reductions of SO₂ and NO_x in the region,
1217 *Atmospheric Chemistry and Physics*, 20, 3107–3134, <https://doi.org/10.5194/acp-20-3107-2020>,
1218 2020.
- 1219 Feng, L., Shen, H., Zhu, Y., Gao, H., and Yao, X.: Insight into Generation and Evolution of Sea-
1220 Salt Aerosols from Field Measurements in Diversified Marine and Coastal Atmospheres, *Sci*
1221 *Rep.*, 7, 41260, <https://doi.org/10.1038/srep41260>, 2017.
- 1222 Ferrare, R., Hair, J., Hostetler, C., Shingler, T., Burton, S. P., Fenn, M., Clayton, M., Scarino, A.
1223 J., Harper, D., Seaman, S., Cook, A., Crosbie, E., Winstead, E., Ziemba, L., Thornhill, L.,
1224 Robinson, C., Moore, R., Vaughan, M., Sorooshian, A., Schlosser, J. S., Liu, H., Zhang, B.,
1225 Diskin, G., DiGangi, J., Nowak, J., Choi, Y., Zuidema, P., and Chellappan, S.: Airborne HSRL-2
1226 measurements of elevated aerosol depolarization associated with non-spherical sea salt, *Frontiers*
1227 *in Remote Sensing*, 4, 01–18, <https://doi.org/10.3389/frsen.2023.1143944>, 2023.
- 1228 Finlayson-Pitts, B. J. and Pitts, J. N.: CHAPTER 9 - Particles in the Troposphere, in: *Chemistry*
1229 *of the Upper and Lower Atmosphere*, edited by: Finlayson-Pitts, B. J. and Pitts, J. N., Academic
1230 Press, San Diego, 349–435, <https://doi.org/10.1016/B978-012257060-5/50011-3>, 2000.
- 1231 Galloway, J. N., Savoie, D. L., Keene, W. C., and Prospero, J. M.: The temporal and spatial
1232 variability of scavenging ratios for NSS sulfate, nitrate, methanesulfonate and sodium in the
1233 Atmosphere over the North Atlantic Ocean, *Atmospheric Environment. Part A. General Topics*,
1234 27, 235–250, [https://doi.org/10.1016/0960-1686\(93\)90354-2](https://doi.org/10.1016/0960-1686(93)90354-2), 1993.
- 1235 Gelaro, R., McCarty, W., Suárez, M. J., Todling, R., Molod, A., Takacs, L., Randles, C. A.,
1236 Darmenov, A., Bosilovich, M. G., Reichle, R., Wargan, K., Coy, L., Cullather, R., Draper, C.,
1237 Akella, S., Buchard, V., Conaty, A., Silva, A. M. da, Gu, W., Kim, G.-K., Koster, R., Lucchesi,
1238 R., Merkova, D., Nielsen, J. E., Partyka, G., Pawson, S., Putman, W., Rienecker, M., Schubert,
1239 S. D., Sienkiewicz, M., and Zhao, B.: The Modern-Era Retrospective Analysis for Research and
1240 Applications, Version 2 (MERRA-2), *Journal of Climate*, 30, 5419–5454,
1241 <https://doi.org/10.1175/JCLI-D-16-0758.1>, 2017.
- 1242 Ghorai, S., Wang, B., Tivanski, A., and Laskin, A.: Hygroscopic Properties of Internally Mixed
1243 Particles Composed of NaCl and Water-Soluble Organic Acids, *Environ. Sci. Technol.*, 48,
1244 2234–2241, <https://doi.org/10.1021/es404727u>, 2014.



- 1245 Grandey, B. S., Stier, P., Wagner, T. M., Grainger, R. G., and Hodges, K. I.: The effect of
1246 extratropical cyclones on satellite-retrieved aerosol properties over ocean, *Geophysical Research*
1247 *Letters*, 38, L13805, <https://doi.org/10.1029/2011GL047703>, 2011.
- 1248 Grassian, V. H.: Chemical Reactions of Nitrogen Oxides on the Surface of Oxide, Carbonate,
1249 Soot, and Mineral Dust Particles: Implications for the Chemical Balance of the Troposphere, *J.*
1250 *Phys. Chem. A*, 106, 860–877, <https://doi.org/10.1021/jp012139h>, 2002.
- 1251 Hanisch, F. and Crowley, J. N.: Heterogeneous reactivity of NO and HNO₃ on mineral dust in
1252 the presence of ozone, *Phys. Chem. Chem. Phys.*, 5, 883–887,
1253 <https://doi.org/10.1039/B211503D>, 2003.
- 1254 Haskins, J. D., Jaeglé, L., Shah, V., Lee, B. H., Lopez-Hilfiker, F. D., Campuzano-Jost, P.,
1255 Schroder, J. C., Day, D. A., Guo, H., Sullivan, A. P., Weber, R., Dibb, J., Campos, T., Jimenez,
1256 J. L., Brown, S. S., and Thornton, J. A.: Wintertime Gas-Particle Partitioning and Speciation of
1257 Inorganic Chlorine in the Lower Troposphere Over the Northeast United States and Coastal
1258 Ocean, *Journal of Geophysical Research: Atmospheres*, 123, 12,897–12,916,
1259 <https://doi.org/10.1029/2018JD028786>, 2018.
- 1260 Hawcroft, M. K., Shaffrey, L. C., Hodges, K. I., and Dacre, H. F.: How much Northern
1261 Hemisphere precipitation is associated with extratropical cyclones?, *Geophysical Research*
1262 *Letters*, 39, L24809, <https://doi.org/10.1029/2012GL053866>, 2012.
- 1263 Hilario, M. R. A., Crosbie, E., Bañaga, P. A., Betito, G., Braun, R. A., Cambaliza, M. O., Corral,
1264 A. F., Cruz, M. T., Dibb, J. E., Lorenzo, G. R., MacDonald, A. B., Robinson, C. E., Shook, M.
1265 A., Simpas, J. B., Stahl, C., Winstead, E., Ziemba, L. D., and Sorooshian, A.: Particulate
1266 Oxalate-To-Sulfate Ratio as an Aqueous Processing Marker: Similarity Across Field Campaigns
1267 and Limitations, *Geophysical Research Letters*, 48, e2021GL096520,
1268 <https://doi.org/10.1029/2021GL096520>, 2021.
- 1269 Hogan, T. F., Liu, M., Ridout, J. A., Peng, M. S., Whitcomb, T. R., Ruston, B. C., Reynolds, C.
1270 A., Eckermann, S. D., Moskaitis, J. R., Baker, N. L., McCORMACK, J. P., Viner, K. C.,
1271 McLAY, J. G., Flatau, M. K., Xu, L., Chen, C., and Chang, S. W.: The Navy Global
1272 Environmental Model, *Oceanography*, 27, 116–125, <https://doi.org/10.5670/oceanog.2014.73>,
1273 2014.
- 1274 Huang, X., Olmez, I., Aras, N. K., and Gordon, G. E.: Emissions of trace elements from motor
1275 vehicles: Potential marker elements and source composition profile, *Atmospheric Environment*,
1276 28, 1385–1391, [https://doi.org/10.1016/1352-2310\(94\)90201-1](https://doi.org/10.1016/1352-2310(94)90201-1), 1994.
- 1277 Hyer, E. J., Reid, J. S., Prins, E. M., Hoffman, J. P., Schmidt, C. C., Miettinen, J. I., and Giglio,
1278 L.: Patterns of fire activity over Indonesia and Malaysia from polar and geostationary satellite
1279 observations, *Atmospheric Research*, 122, 504–519,
1280 <https://doi.org/10.1016/j.atmosres.2012.06.011>, 2013.
- 1281 J. S. Reid, E. J. Hyer, E. M. Prins, D. L. Westphal, J. Zhang, J. Wang, S. A. Christopher, C. A.
1282 Curtis, C. C. Schmidt, D. P. Eleuterio, K. A. Richardson, and J. P. Hoffman: Global Monitoring
1283 and Forecasting of Biomass-Burning Smoke: Description of and Lessons From the Fire Locating



- 1284 and Modeling of Burning Emissions (FLAMBE) Program, *IEEE Journal of Selected Topics in*
1285 *Applied Earth Observations and Remote Sensing*, 2, 144–162,
1286 <https://doi.org/10.1109/JSTARS.2009.2027443>, 2009.
- 1287 Jaffe, D. A., O’Neill, S. M., Larkin, N. K., Holder, A. L., Peterson, D. L., Halofsky, J. E., and
1288 Rappold, A. G.: Wildfire and prescribed burning impacts on air quality in the United States,
1289 *Journal of the Air & Waste Management Association*, 70, 583–615,
1290 <https://doi.org/10.1080/10962247.2020.1749731>, 2020.
- 1291 Jing, B., Peng, C., Wang, Y., Liu, Q., Tong, S., Zhang, Y., and Ge, M.: Hygroscopic properties
1292 of potassium chloride and its internal mixtures with organic compounds relevant to biomass
1293 burning aerosol particles, *Sci Rep*, 7, 43572, <https://doi.org/10.1038/srep43572>, 2017.
- 1294 Kacenelenbogen, M. S. F., Tan, Q., Burton, S. P., Hasekamp, O. P., Froyd, K. D., Shinozuka, Y.,
1295 Beyersdorf, A. J., Ziemba, L., Thornhill, K. L., Dibb, J. E., Shingler, T., Sorooshian, A.,
1296 Espinosa, R. W., Martins, V., Jimenez, J. L., Campuzano-Jost, P., Schwarz, J. P., Johnson, M. S.,
1297 Redemann, J., and Schuster, G. L.: Identifying chemical aerosol signatures using optical
1298 suborbital observations: how much can optical properties tell us about aerosol composition?,
1299 *Atmospheric Chemistry and Physics*, 22, 3713–3742, <https://doi.org/10.5194/acp-22-3713-2022>,
1300 2022.
- 1301 Kavouras, I. G., Nikolich, G., Etyemezian, V., DuBois, D. W., King, J., and Shafer, D.: In situ
1302 observations of soil minerals and organic matter in the early phases of prescribed fires, *Journal of*
1303 *Geophysical Research: Atmospheres*, 117, D12313, <https://doi.org/10.1029/2011JD017420>,
1304 2012.
- 1305 Keene, W. C. and Savoie, D. L.: The pH of deliquesced sea-salt aerosol in polluted marine air,
1306 *Geophysical Research Letters*, 25, 2181–2184, <https://doi.org/10.1029/98GL01591>, 1998.
- 1307 Keene, W. C., Pszenny, A. A. P., Jacob, D. J., Duce, R. A., Galloway, J. N., Schultz-Tokos, J. J.,
1308 Sievering, H., and Boatman, J. F.: The geochemical cycling of reactive chlorine through the
1309 marine troposphere, *Global Biogeochemical Cycles*, 4, 407–430,
1310 <https://doi.org/10.1029/GB004i004p00407>, 1990.
- 1311 Keene, W. C., Pszenny, A. A. P., Maben, J. R., Stevenson, E., and Wall, A.: Closure evaluation
1312 of size-resolved aerosol pH in the New England coastal atmosphere during summer, *Journal of*
1313 *Geophysical Research: Atmospheres*, 109, D23307, <https://doi.org/10.1029/2004JD004801>,
1314 2004.
- 1315 Keene, W. C., Stutz, J., Pszenny, A. A. P., Maben, J. R., Fischer, E. V., Smith, A. M., von
1316 Glasow, R., Pechtl, S., Sive, B. C., and Varner, R. K.: Inorganic chlorine and bromine in coastal
1317 New England air during summer, *Journal of Geophysical Research: Atmospheres*, 112, D10S12,
1318 <https://doi.org/10.1029/2006JD007689>, 2007.
- 1319 Keene, William C., Khalil, M. A. K., Erickson III, David J., McCulloch, A., Graedel, T. E.,
1320 Lobert, J. M., Aucott, M. L., Gong, S. L., Harper, D. B., Kleiman, G., Midgley, P., Moore, R.
1321 M., Seuzaret, C., Sturges, W. T., Benkovitz, C. M., Koropalov, V., Barrie, L. A., and Li, Y. F.:
1322 Composite global emissions of reactive chlorine from anthropogenic and natural sources:



- 1323 Reactive Chlorine Emissions Inventory, *Journal of Geophysical Research: Atmospheres*, 104,
1324 8429–8440, <https://doi.org/10.1029/1998JD100084>, 1999.
- 1325 Keim, B. D., Meeker, L. D., and Slater, J. F.: Manual synoptic climate classification for the east
1326 coast of New England (USA) with an application to PM_{2.5} concentration, *Climate Research*, 28,
1327 143–153, <https://doi.org/10.3354/cr028143>, 2005.
- 1328 Kerminen, V.-M., Teinilä, K., Hillamo, R., and Pakkanen, T.: Substitution of chloride in sea-salt
1329 particles by inorganic and organic anions, *Journal of Aerosol Science*, 29, 929–942,
1330 [https://doi.org/10.1016/S0021-8502\(98\)00002-0](https://doi.org/10.1016/S0021-8502(98)00002-0), 1998.
- 1331 Knipping, E. M. and Dabdub, D.: Impact of Chlorine Emissions from Sea-Salt Aerosol on
1332 Coastal Urban Ozone, *Environ. Sci. Technol.*, 37, 275–284, <https://doi.org/10.1021/es025793z>,
1333 2003.
- 1334 Kong, S., Wen, B., Chen, K., Yin, Y., Li, L., Li, Q., Yuan, L., Li, X., and Sun, X.: Ion chemistry
1335 for atmospheric size-segregated aerosol and depositions at an offshore site of Yangtze River
1336 Delta region, China, *Atmospheric Research*, 147–148, 205–226,
1337 <https://doi.org/10.1016/j.atmosres.2014.05.018>, 2014.
- 1338 Kuklinska, K., Wolska, L., and Namiesnik, J.: Air quality policy in the U.S. and the EU – a
1339 review, *Atmospheric Pollution Research*, 6, 129–137, <https://doi.org/10.5094/APR.2015.015>,
1340 2015.
- 1341 Lamberg, H., Nuutinen, K., Tissari, J., Ruusunen, J., Yli-Pirilä, P., Sippula, O., Tapanainen, M.,
1342 Jalava, P., Makkonen, U., Teinilä, K., Saarnio, K., Hillamo, R., Hirvonen, M.-R., and Jokiniemi,
1343 J.: Physicochemical characterization of fine particles from small-scale wood combustion,
1344 *Atmospheric Environment*, 45, 7635–7643, <https://doi.org/10.1016/j.atmosenv.2011.02.072>,
1345 2011.
- 1346 Laskin, A., Moffet, R. C., Gilles, M. K., Fast, J. D., Zaveri, R. A., Wang, B., Nigge, P., and
1347 Shutthanandan, J.: Tropospheric chemistry of internally mixed sea salt and organic particles:
1348 Surprising reactivity of NaCl with weak organic acids, *Journal of Geophysical Research:*
1349 *Atmospheres*, 117, D15302, <https://doi.org/10.1029/2012JD017743>, 2012.
- 1350 Li, J., Pósfai, M., Hobbs, P. V., and Buseck, P. R.: Individual aerosol particles from biomass
1351 burning in southern Africa: 2, Compositions and aging of inorganic particles, *Journal of*
1352 *Geophysical Research: Atmospheres*, 108, 8484, <https://doi.org/10.1029/2002JD002310>, 2003.
- 1353 Lippmann, M.: HEALTH EFFECTS OF OZONE A Critical Review, *JAPCA*, 39, 672–695,
1354 <https://doi.org/10.1080/08940630.1989.10466554>, 1989.
- 1355 Luria, M., Van Valin, C. C., Galloway, J. N., Keene, W. C., Wellman, D. L., Sievering, H., and
1356 Boatman, J. F.: The relationship between dimethyl sulfide and particulate sulfate in the mid-
1357 atlantic ocean atmosphere, *Atmospheric Environment*, 23, 139–147,
1358 [https://doi.org/10.1016/0004-6981\(89\)90106-6](https://doi.org/10.1016/0004-6981(89)90106-6), 1989.



- 1359 Lynch, P., Reid, J. S., Westphal, D. L., Zhang, J., Hogan, T. F., Hyer, E. J., Curtis, C. A., Hegg,
1360 D. A., Shi, Y., Campbell, J. R., Rubin, J. I., Sessions, W. R., Turk, F. J., and Walker, A. L.: An
1361 11-year global gridded aerosol optical thickness reanalysis (v1.0) for atmospheric and climate
1362 sciences, *Geoscientific Model Development*, 9, 1489–1522, [https://doi.org/10.5194/gmd-9-1489-](https://doi.org/10.5194/gmd-9-1489-2016)
1363 2016, 2016.
- 1364 Mardi, A. H., Dadashazar, H., Painemal, D., Shingler, T., Seaman, S. T., Fenn, M. A., Hostetler,
1365 C. A., and Sorooshian, A.: Biomass Burning Over the United States East Coast and Western
1366 North Atlantic Ocean: Implications for Clouds and Air Quality, *Journal of Geophysical*
1367 *Research: Atmospheres*, 126, e2021JD034916, <https://doi.org/10.1029/2021JD034916>, 2021.
- 1368 Maudlin, L. C., Wang, Z., Jonsson, H. H., and Sorooshian, A.: Impact of wildfires on size-
1369 resolved aerosol composition at a coastal California site, *Atmospheric Environment*, 119, 59–68,
1370 <https://doi.org/10.1016/j.atmosenv.2015.08.039>, 2015.
- 1371 McCarty, J. L., Justice, C. O., and Korontzi, S.: Agricultural burning in the Southeastern United
1372 States detected by MODIS, *Remote Sensing of Environment*, 108, 151–162,
1373 <https://doi.org/10.1016/j.rse.2006.03.020>, 2007.
- 1374 McNaughton, C. S., Clarke, A. D., Howell, S. G., Pinkerton, M., Anderson, B., Thornhill, L.,
1375 Hudgins, C., Winstead, E., Dibb, J. E., Scheuer, E., and Maring, H.: Results from the DC-8 Inlet
1376 Characterization Experiment (DICE): Airborne Versus Surface Sampling of Mineral Dust and
1377 Sea Salt Aerosols, *Aerosol Science and Technology*, 41, 136–159,
1378 <https://doi.org/10.1080/02786820601118406>, 2007.
- 1379 Moffet, R. C., Desyaterik, Y., Hopkins, R. J., Tivanski, A. V., Gilles, M. K., Wang, Y.,
1380 Shutthanandan, V., Molina, L. T., Abraham, R. G., Johnson, K. S., Mugica, V., Molina, M. J.,
1381 Laskin, A., and Prather, K. A.: Characterization of aerosols containing Zn, Pb, and Cl from an
1382 industrial region of Mexico City, *Environ Sci Technol*, 42, 7091–7097,
1383 <https://doi.org/10.1021/es7030483>, 2008.
- 1384 Molina, M. J. and Rowland, F. S.: Stratospheric sink for chlorofluoromethanes: chlorine atom-
1385 catalysed destruction of ozone, *Nature*, 249, 810–812, <https://doi.org/10.1038/249810a0>, 1974.
- 1386 Naeher, L. P., Smith, K. R., Leaderer, B. P., Neufeld, L., and Mage, D. T.: Carbon Monoxide As
1387 a Tracer for Assessing Exposures to Particulate Matter in Wood and Gas Cookstove Households
1388 of Highland Guatemala, *Environ. Sci. Technol.*, 35, 575–581, <https://doi.org/10.1021/es991225g>,
1389 2001.
- 1390 Nolte, C., Bhave, P., Arnold, J., Dennis, R., Zhang, K., and Wexler, A.: Modeling urban and
1391 regional aerosols—Application of the CMAQ-UCD Aerosol Model to Tampa, a coastal urban
1392 site, *Atmospheric Environment*, 42, 3179–3191, <https://doi.org/10.1016/j.atmosenv.2007.12.059>,
1393 2008.
- 1394 Nuvolone, D., Petri, D., and Voller, F.: The effects of ozone on human health, *Environ Sci Pollut*
1395 *Res*, 25, 8074–8088, <https://doi.org/10.1007/s11356-017-9239-3>, 2018.



- 1396 Ondov, J. M., Choquette, C. E., Zoller, W. H., Gordon, G. E., Biermann, A. H., and Heft, R. E.:
1397 Atmospheric behavior of trace elements on particles emitted from a coal-fired power plant,
1398 Atmospheric Environment, 23, 2193–2204, [https://doi.org/10.1016/0004-6981\(89\)90181-9](https://doi.org/10.1016/0004-6981(89)90181-9),
1399 1989.
- 1400 Ooki, A. and Uematsu, M.: Chemical interactions between mineral dust particles and acid gases
1401 during Asian dust events, Journal of Geophysical Research: Atmospheres, 110,
1402 <https://doi.org/10.1029/2004JD004737>, 2005.
- 1403 Ooki, A., Uematsu, M., Miura, K., and Nakae, S.: Sources of sodium in atmospheric fine
1404 particles, Atmospheric Environment, 36, 4367–4374, [https://doi.org/10.1016/S1352-](https://doi.org/10.1016/S1352-2310(02)00341-2)
1405 2310(02)00341-2, 2002.
- 1406 Osthoff, H. D., Roberts, J. M., Ravishankara, A. R., Williams, E. J., Lerner, B. M., Sommariva,
1407 R., Bates, T. S., Coffman, D., Quinn, P. K., Dibb, J. E., Stark, H., Burkholder, J. B., Talukdar, R.
1408 K., Meagher, J., Fehsenfeld, F. C., and Brown, S. S.: High levels of nitryl chloride in the polluted
1409 subtropical marine boundary layer, Nature Geoscience, 1, 324–328,
1410 <https://doi.org/10.1038/ngeo177>, 2008.
- 1411 Painemal, D., Corral, A. F., Sorooshian, A., Brunke, M. A., Chellappan, S., Afzali Goroooh, V.,
1412 Ham, S.-H., O’Neill, L., Smith Jr., W. L., Tselioudis, G., Wang, H., Zeng, X., and Zuidema, P.:
1413 An Overview of Atmospheric Features Over the Western North Atlantic Ocean and North
1414 American East Coast—Part 2: Circulation, Boundary Layer, and Clouds, Journal of Geophysical
1415 Research: Atmospheres, 126, e2020JD033423, <https://doi.org/10.1029/2020JD033423>, 2021.
- 1416 Palmer, T. Y.: Large fire winds, gases and smoke, Atmospheric Environment, 15, 2079–2090,
1417 [https://doi.org/10.1016/0004-6981\(81\)90241-9](https://doi.org/10.1016/0004-6981(81)90241-9), 1981.
- 1418 Panagi, M., Fleming, Z. L., Monks, P. S., Ashfold, M. J., Wild, O., Hollaway, M., Zhang, Q.,
1419 Squires, F. A., and Vande Hey, J. D.: Investigating the regional contributions to air pollution in
1420 Beijing: a dispersion modelling study using CO as a tracer, Atmospheric Chemistry and Physics,
1421 20, 2825–2838, <https://doi.org/10.5194/acp-20-2825-2020>, 2020.
- 1422 Park, S.-S., Sim, S. Y., Bae, M.-S., and Schauer, J. J.: Size distribution of water-soluble
1423 components in particulate matter emitted from biomass burning, Atmospheric Environment, 73,
1424 62–72, <https://doi.org/10.1016/j.atmosenv.2013.03.025>, 2013.
- 1425 Parungo, F. P., Nagamoto, C. T., Madel, R., Rosinski, J., and Haagenson, P. L.: Marine aerosols
1426 in pacific upwelling regions, Journal of Aerosol Science, 18, 277–290,
1427 [https://doi.org/10.1016/0021-8502\(87\)90023-1](https://doi.org/10.1016/0021-8502(87)90023-1), 1987.
- 1428 Pechtl, S. and von Glasow, R.: Reactive chlorine in the marine boundary layer in the outflow of
1429 polluted continental air: A model study, Geophysical Research Letters, 34, L11813,
1430 <https://doi.org/10.1029/2007GL029761>, 2007.
- 1431 Perry, K. D., Cahill, T. A., Eldred, R. A., Dutcher, D. D., and Gill, T. E.: Long-range transport of
1432 North African dust to the eastern United States, Journal of Geophysical Research: Atmospheres,
1433 102, 11225–11238, <https://doi.org/10.1029/97JD00260>, 1997.



- 1434 Popovicheva, O., Kistler, M., Kireeva, E., Persiantseva, N., Timofeev, M., Kopeikin, V., and
1435 Kasper-Giebl, A.: Physicochemical characterization of smoke aerosol during large-scale
1436 wildfires: Extreme event of August 2010 in Moscow, *Atmospheric Environment*, 96, 405–414,
1437 <https://doi.org/10.1016/j.atmosenv.2014.03.026>, 2014.
- 1438 Prospero, J. M.: Saharan Dust Transport Over the North Atlantic Ocean and Mediterranean: An
1439 Overview, in: *The Impact of Desert Dust Across the Mediterranean*, edited by: Guerzoni, S. and
1440 Chester, R., Springer Netherlands, Dordrecht, 133–151, https://doi.org/10.1007/978-94-017-3354-0_13, 1996.
- 1442 Prospero, J. M.: Long-term measurements of the transport of African mineral dust to the
1443 southeastern United States: Implications for regional air quality, *Journal of Geophysical
1444 Research: Atmospheres*, 104, 15917–15927, <https://doi.org/10.1029/1999JD900072>, 1999.
- 1445 Quinn, P. K. and Bates, T. S.: Regional aerosol properties: Comparisons of boundary layer
1446 measurements from ACE 1, ACE 2, Aerosols99, INDOEX, ACE Asia, TARFOX, and NEAQS,
1447 *Journal of Geophysical Research: Atmospheres*, 110, D14202,
1448 <https://doi.org/10.1029/2004JD004755>, 2005.
- 1449 Randles, C. A., Russell, L. M., and Ramaswamy, V.: Hygroscopic and optical properties of
1450 organic sea salt aerosol and consequences for climate forcing, *Geophysical Research Letters*, 31,
1451 L16108, <https://doi.org/10.1029/2004GL020628>, 2004.
- 1452 Rastogi, N., Agnihotri, R., Sawlani, R., Patel, A., Babu, S. S., and Satish, R.: Chemical and
1453 isotopic characteristics of PM10 over the Bay of Bengal: Effects of continental outflow on a
1454 marine environment, *Science of The Total Environment*, 726, 138438,
1455 <https://doi.org/10.1016/j.scitotenv.2020.138438>, 2020.
- 1456 Reid, J. S., Jonsson, H. H., Smith, M. H., and Smirnov, A.: Evolution of the vertical profile and
1457 flux of large sea-salt particles in a coastal zone, *Journal of Geophysical Research: Atmospheres*,
1458 106, 12039–12053, <https://doi.org/10.1029/2000JD900848>, 2001.
- 1459 Riedel, T. P., Wolfe, G. M., Danas, K. T., Gilman, J. B., Kuster, W. C., Bon, D. M., Vlasenko,
1460 A., Li, S.-M., Williams, E. J., Lerner, B. M., Veres, P. R., Roberts, J. M., Holloway, J. S., Lefer,
1461 B., Brown, S. S., and Thornton, J. A.: An MCM modeling study of nitryl chloride (ClNO₂)
1462 impacts on oxidation, ozone production and nitrogen oxide partitioning in polluted continental
1463 outflow, *Atmospheric Chemistry and Physics*, 14, 3789–3800, <https://doi.org/10.5194/acp-14-3789-2014>, 2014.
- 1465 Roberts, J. M., Osthoff, H. D., Brown, S. S., and Ravishankara, A. R.: N₂O₅ Oxidizes Chloride
1466 to Cl₂ in Acidic Atmospheric Aerosol, *Science*, 321, 1059–1059,
1467 <https://doi.org/10.1126/science.1158777>, 2008.
- 1468 Robinson, A. L., Donahue, N. M., Shrivastava, M. K., Weitkamp, E. A., Sage, A. M., Grieshop,
1469 A. P., Lane, T. E., Pierce, J. R., and Pandis, S. N.: Rethinking Organic Aerosols: Semivolatile
1470 Emissions and Photochemical Aging, *Science*, 315, 1259–1262,
1471 <https://doi.org/10.1126/science.1133061>, 2007.



- 1472 Saide, P. E., Carmichael, G. R., Spak, S. N., Gallardo, L., Osses, A. E., Mena-Carrasco, M. A.,
1473 and Pagowski, M.: Forecasting urban PM₁₀ and PM_{2.5} pollution episodes in very stable
1474 nocturnal conditions and complex terrain using WRF–Chem CO tracer model, *Atmospheric*
1475 *Environment*, 45, 2769–2780, <https://doi.org/10.1016/j.atmosenv.2011.02.001>, 2011.
- 1476 Santschi, Ch. and Rossi, M. J.: Uptake of CO₂, SO₂, HNO₃ and HCl on Calcite (CaCO₃) at 300
1477 K: Mechanism and the Role of Adsorbed Water, *J. Phys. Chem. A*, 110, 6789–6802,
1478 <https://doi.org/10.1021/jp056312b>, 2006.
- 1479 Savoie, D. L., Arimoto, R., Keene, W. C., Prospero, J. M., Duce, R. A., and Galloway, J. N.:
1480 Marine biogenic and anthropogenic contributions to non-sea-salt sulfate in the marine boundary
1481 layer over the North Atlantic Ocean, *Journal of Geophysical Research: Atmospheres*, 107, AAC
1482 3-1-AAC 3-21, <https://doi.org/10.1029/2001JD000970>, 2002.
- 1483 Schlosser, J. S., Braun, R. A., Bradley, T., Dadashazar, H., MacDonald, A. B., Aldhaif, A. A.,
1484 Aghdam, M. A., Mardi, A. H., Xian, P., and Sorooshian, A.: Analysis of aerosol composition
1485 data for western United States wildfires between 2005 and 2015: Dust emissions, chloride
1486 depletion, and most enhanced aerosol constituents, *Journal of Geophysical Research:*
1487 *Atmospheres*, 122, 8951–8966, <https://doi.org/10.1002/2017JD026547>, 2017.
- 1488 Schroder, J. C., Campuzano-Jost, P., Day, D. A., Shah, V., Larson, K., Sommers, J. M., Sullivan,
1489 A. P., Campos, T., Reeves, J. M., Hills, A., Hornbrook, R. S., Blake, N. J., Scheuer, E., Guo, H.,
1490 Fibiger, D. L., McDuffie, E. E., Hayes, P. L., Weber, R. J., Dibb, J. E., Apel, E. C., Jaeglé, L.,
1491 Brown, S. S., Thornton, J. A., and Jimenez, J. L.: Sources and Secondary Production of Organic
1492 Aerosols in the Northeastern United States during WINTER, *Journal of Geophysical Research:*
1493 *Atmospheres*, 123, 7771–7796, <https://doi.org/10.1029/2018JD028475>, 2018.
- 1494 Seinfeld, J. H. and Pandis, S. N.: *Atmospheric Chemistry and Physics: From Air Pollution to*
1495 *Climate Change*, John Wiley & Sons, 1146 pp., 2016.
- 1496 Sherwen, T., Schmidt, J. A., Evans, M. J., Carpenter, L. J., Großmann, K., Eastham, S. D., Jacob,
1497 D. J., Dix, B., Koenig, T. K., Sinreich, R., Ortega, I., Volkamer, R., Saiz-Lopez, A., Prados-
1498 Roman, C., Mahajan, A. S., and Ordóñez, C.: Global impacts of tropospheric halogens (Cl, Br, I)
1499 on oxidants and composition in GEOS-Chem, *Atmospheric Chemistry and Physics*, 16, 12239–
1500 12271, <https://doi.org/10.5194/acp-16-12239-2016>, 2016.
- 1501 Shingler, T., Dey, S., Sorooshian, A., Brechtel, F. J., Wang, Z., Metcalf, A., Coggon, M.,
1502 Mülmenstädt, J., Russell, L. M., Jonsson, H. H., and Seinfeld, J. H.: Characterisation and
1503 airborne deployment of a new counterflow virtual impactor inlet, *Atmospheric Measurement*
1504 *Techniques*, 5, 1259–1269, <https://doi.org/10.5194/amt-5-1259-2012>, 2012.
- 1505 Shinozuka, Y., Clarke, A. D., Howell, S. G., Kapustin, V. N., and Huebert, B. J.: Sea-salt vertical
1506 profiles over the Southern and tropical Pacific oceans: Microphysics, optical properties, spatial
1507 variability, and variations with wind speed, *Journal of Geophysical Research: Atmospheres*, 109,
1508 D24201, <https://doi.org/10.1029/2004JD004975>, 2004.



- 1509 Singh, H. B. and Kasting, J. F.: Chlorine-hydrocarbon photochemistry in the marine troposphere
1510 and lower stratosphere, *Journal of Atmospheric Chemistry*, 7, 261–285,
1511 <https://doi.org/10.1007/BF00130933>, 1988.
- 1512 Solomon, S., Stone, K., Yu, P., Murphy, D. M., Kinnison, D., Ravishankara, A. R., and Wang,
1513 P.: Chlorine activation and enhanced ozone depletion induced by wildfire aerosol, *Nature*, 615,
1514 259–264, <https://doi.org/10.1038/s41586-022-05683-0>, 2023.
- 1515 Sorooshian, A., Brechtel, F. J., Ma, Y., Weber, R. J., Corless, A., Flagan, R. C., and Seinfeld, J.
1516 H.: Modeling and Characterization of a Particle-into-Liquid Sampler (PILS), *Aerosol Science
1517 and Technology*, 40, 396–409, <https://doi.org/10.1080/02786820600632282>, 2006.
- 1518 Sorooshian, A., Murphy, S. M., Hersey, S., Bahreini, R., Jonsson, H., Flagan, R. C., and
1519 Seinfeld, J. H.: Constraining the contribution of organic acids and AMS m/z 44 to the organic
1520 aerosol budget: On the importance of meteorology, aerosol hygroscopicity, and region,
1521 *Geophysical Research Letters*, 37, L21807, <https://doi.org/10.1029/2010GL044951>, 2010.
- 1522 Sorooshian, A., Csavina, J., Shingler, T., Dey, S., Brechtel, F. J., Sáez, A. E., and Betterton, E.
1523 A.: Hygroscopic and Chemical Properties of Aerosols Collected near a Copper Smelter:
1524 Implications for Public and Environmental Health, *Environ. Sci. Technol.*, 46, 9473–9480,
1525 <https://doi.org/10.1021/es302275k>, 2012.
- 1526 Sorooshian, A., Anderson, B., Bauer, S. E., Braun, R. A., Cairns, B., Crosbie, E., Dadashazar,
1527 H., Diskin, G., Ferrare, R., Flagan, R. C., Hair, J., Hostetler, C., Jonsson, H. H., Kleb, M. M.,
1528 Liu, H., MacDonald, A. B., McComiskey, A., Moore, R., Painemal, D., Russell, L. M., Seinfeld,
1529 J. H., Shook, M., Smith, W. L., Thornhill, K., Tselioudis, G., Wang, H., Zeng, X., Zhang, B.,
1530 Ziemba, L., and Zuidema, P.: Aerosol–Cloud–Meteorology Interaction Airborne Field
1531 Investigations: Using Lessons Learned from the U.S. West Coast in the Design of ACTIVATE
1532 off the U.S. East Coast, *Bulletin of the American Meteorological Society*, 100, 1511–1528,
1533 <https://doi.org/10.1175/BAMS-D-18-0100.1>, 2019.
- 1534 Sorooshian, A., Corral, A. F., Braun, R. A., Cairns, B., Crosbie, E., Ferrare, R., Hair, J., Kleb, M.
1535 M., Hossein Mardi, A., Maring, H., McComiskey, A., Moore, R., Painemal, D., Scarino, A. J.,
1536 Schlosser, J., Shingler, T., Shook, M., Wang, H., Zeng, X., Ziemba, L., and Zuidema, P.:
1537 Atmospheric Research Over the Western North Atlantic Ocean Region and North American East
1538 Coast: A Review of Past Work and Challenges Ahead, *Journal of Geophysical Research:
1539 Atmospheres*, 125, e2019JD031626, <https://doi.org/10.1029/2019JD031626>, 2020.
- 1540 Sorooshian, A., Alexandrov, M. D., Bell, A. D., Bennett, R., Betito, G., Burton, S. P.,
1541 Buzanowicz, M. E., Cairns, B., Chemyakin, E. V., Chen, G., Choi, Y., Collister, B. L., Cook, A.
1542 L., Corral, A. F., Crosbie, E. C., van Diedenhoven, B., DiGangi, J. P., Diskin, G. S., Dmitrovic,
1543 S., Edwards, E.-L., Fenn, M. A., Ferrare, R. A., van Gilst, D., Hair, J. W., Harper, D. B., Hilario,
1544 M. R. A., Hostetler, C. A., Jester, N., Jones, M., Kirschler, S., Kleb, M. M., Kusterer, J. M.,
1545 Leavor, S., Lee, J. W., Liu, H., McCauley, K., Moore, R. H., Nied, J., Notari, A., Nowak, J. B.,
1546 Painemal, D., Phillips, K. E., Robinson, C. E., Scarino, A. J., Schlosser, J. S., Seaman, S. T.,
1547 Seethala, C., Shingler, T. J., Shook, M. A., Sinclair, K. A., Smith Jr., W. L., Spangenberg, D. A.,
1548 Stamnes, S. A., Thornhill, K. L., Voigt, C., Vömel, H., Wasilewski, A. P., Wang, H., Winstead,



- 1549 E. L., Zeider, K., Zeng, X., Zhang, B., Ziemba, L. D., and Zuidema, P.: Spatially coordinated
1550 airborne data and complementary products for aerosol, gas, cloud, and meteorological studies:
1551 the NASA ACTIVATE dataset, *Earth System Science Data*, 15, 3419–3472,
1552 <https://doi.org/10.5194/essd-15-3419-2023>, 2023.
- 1553 Su, B., Wang, T., Zhang, G., Liang, Y., Lv, C., Hu, Y., Li, L., Zhou, Z., Wang, X., and Bi, X.: A
1554 review of atmospheric aging of sea spray aerosols: Potential factors affecting chloride depletion,
1555 *Atmospheric Environment*, 290, 119365, <https://doi.org/10.1016/j.atmosenv.2022.119365>, 2022.
- 1556 Sullivan, A. P., Guo, H., Schroder, J. C., Campuzano-Jost, P., Jimenez, J. L., Campos, T., Shah,
1557 V., Jaeglé, L., Lee, B. H., Lopez-Hilfiker, F. D., Thornton, J. A., Brown, S. S., and Weber, R. J.:
1558 Biomass Burning Markers and Residential Burning in the WINTER Aircraft Campaign, *Journal*
1559 *of Geophysical Research: Atmospheres*, 124, 1846–1861,
1560 <https://doi.org/10.1029/2017JD028153>, 2019.
- 1561 Sullivan, R. C., Guazzotti, S. A., Sodeman, D. A., and Prather, K. A.: Direct observations of the
1562 atmospheric processing of Asian mineral dust, *Atmospheric Chemistry and Physics*, 7, 1213–
1563 1236, <https://doi.org/10.5194/acp-7-1213-2007>, 2007.
- 1564 Takegawa, N., Miyakawa, T., Kawamura, K., and Kondo, Y.: Contribution of Selected
1565 Dicarboxylic and ω -Oxocarboxylic Acids in Ambient Aerosol to the m/z 44 Signal of an
1566 Aerodyne Aerosol Mass Spectrometer, *Aerosol Science and Technology*, 41, 418–437,
1567 <https://doi.org/10.1080/02786820701203215>, 2007.
- 1568 Tanaka, P. L., Riemer, D. D., Chang, S., Yarwood, G., McDonald-Buller, E. C., Apel, E. C.,
1569 Orlando, J. J., Silva, P. J., Jimenez, J. L., Canagaratna, M. R., Neece, J. D., Mullins, C. B., and
1570 Allen, D. T.: Direct evidence for chlorine-enhanced urban ozone formation in Houston, Texas,
1571 *Atmospheric Environment*, 37, 1393–1400, [https://doi.org/10.1016/S1352-2310\(02\)01007-5](https://doi.org/10.1016/S1352-2310(02)01007-5),
1572 2003.
- 1573 Tang, I. N., Tridico, A. C., and Fung, K. H.: Thermodynamic and optical properties of sea salt
1574 aerosols, *Journal of Geophysical Research: Atmospheres*, 102, 23269–23275,
1575 <https://doi.org/10.1029/97JD01806>, 1997.
- 1576 Tang, M., Guo, L., Bai, Y., Huang, R.-J., Wu, Z., Wang, Z., Zhang, G., Ding, X., Hu, M., and
1577 Wang, X.: Impacts of methanesulfonate on the cloud condensation nucleation activity of sea salt
1578 aerosol, *Atmospheric Environment*, 201, 13–17, <https://doi.org/10.1016/j.atmosenv.2018.12.034>,
1579 2019.
- 1580 Thornhill, K. L., Anderson, B. E., Barrick, J. D. W., Bagwell, D. R., Friesen, R., and Lenschow,
1581 D. H.: Air motion intercomparison flights during Transport and Chemical Evolution in the
1582 Pacific (TRACE-P)/ACE-ASIA, *Journal of Geophysical Research: Atmospheres*, 108, 8783,
1583 <https://doi.org/10.1029/2002JD003108>, 2003.
- 1584 Thornton, J. A., Kercher, J. P., Riedel, T. P., Wagner, N. L., Cozic, J., Holloway, J. S., Dubé, W.
1585 P., Wolfe, G. M., Quinn, P. K., Middlebrook, A. M., Alexander, B., and Brown, S. S.: A large
1586 atomic chlorine source inferred from mid-continental reactive nitrogen chemistry, *Nature*, 464,
1587 271–274, <https://doi.org/10.1038/nature08905>, 2010.



- 1588 Toole, D. A. and Siegel, D. A.: Light-driven cycling of dimethylsulfide (DMS) in the Sargasso
1589 Sea: Closing the loop, *Geophysical Research Letters*, 31, L09308,
1590 <https://doi.org/10.1029/2004GL019581>, 2004.
- 1591 Ullerstam, M., Vogt, R., Langer, S., and Ljungström, E.: The kinetics and mechanism of SO₂
1592 oxidation by O₃ on mineral dust, *Phys. Chem. Chem. Phys.*, 4, 4694–4699,
1593 <https://doi.org/10.1039/B203529B>, 2002.
- 1594 Vallina, S. M. and Simó, R.: Strong Relationship Between DMS and the Solar Radiation Dose
1595 over the Global Surface Ocean, *Science*, 315, 506–508, <https://doi.org/10.1126/science.1133680>,
1596 2007.
- 1597 Van Rooy, P., Drover, R., Cress, T., Michael, C., Purvis-Roberts, K. L., Silva, P. J., Nee, M. J.,
1598 and Cocker, D.: Methanesulfonic acid and sulfuric acid Aerosol Formed through oxidation of
1599 reduced sulfur compounds in a humid environment, *Atmospheric Environment*, 261, 118504,
1600 <https://doi.org/10.1016/j.atmosenv.2021.118504>, 2021.
- 1601 Wittig, V. E., Ainsworth, E. A., Naidu, S. L., Karnosky, D. F., and Long, S. P.: Quantifying the
1602 impact of current and future tropospheric ozone on tree biomass, growth, physiology and
1603 biochemistry: a quantitative meta-analysis, *Global Change Biology*, 15, 396–424,
1604 <https://doi.org/10.1111/j.1365-2486.2008.01774.x>, 2009.
- 1605 Wu, Y., Han, Z., Nazmi, C., Gross, B., and Moshary, F.: A trans-Pacific Asian dust episode and
1606 its impacts to air quality in the east coast of U.S., *Atmospheric Environment*, 106, 358–368,
1607 <https://doi.org/10.1016/j.atmosenv.2015.02.013>, 2015.
- 1608 Yan, J., Jung, J., Zhang, M., Bianchi, F., Tham, Y. J., Xu, S., Lin, Q., Zhao, S., Li, L., and Chen,
1609 L.: Uptake selectivity of methanesulfonic acid (MSA) on fine particles over polynya regions of
1610 the Ross Sea, Antarctica, *Atmospheric Chemistry and Physics*, 20, 3259–3271,
1611 <https://doi.org/10.5194/acp-20-3259-2020>, 2020.
- 1612 Yao, X. and Zhang, L.: Chemical processes in sea-salt chloride depletion observed at a Canadian
1613 rural coastal site, *Atmospheric Environment*, 46, 189–194,
1614 <https://doi.org/10.1016/j.atmosenv.2011.09.081>, 2012.
- 1615 Yokelson, R. J., Crouse, J. D., DeCarlo, P. F., Karl, T., Urbanski, S., Atlas, E., Campos, T.,
1616 Shinozuka, Y., Kapustin, V., Clarke, A. D., Weinheimer, A., Knapp, D. J., Montzka, D. D.,
1617 Holloway, J., Weibring, P., Flocke, F., Zheng, W., Toohey, D., Wennberg, P. O., Wiedinmyer,
1618 C., Mauldin, L., Fried, A., Richter, D., Walega, J., Jimenez, J. L., Adachi, K., Buseck, P. R.,
1619 Hall, S. R., and Shetter, R.: Emissions from biomass burning in the Yucatan, *Atmospheric
1620 Chemistry and Physics*, 9, 5785–5812, <https://doi.org/10.5194/acp-9-5785-2009>, 2009.
- 1621 Young, A. H., Keene, W. C., Pszenny, A. A. P., Sander, R., Thornton, J. A., Riedel, T. P., and
1622 Maben, J. R.: Phase partitioning of soluble trace gases with size-resolved aerosols in near-surface
1623 continental air over northern Colorado, USA, during winter, *Journal of Geophysical Research:
1624 Atmospheres*, 118, 9414–9427, <https://doi.org/10.1002/jgrd.50655>, 2013.



- 1625 Young, C. J., Washenfelder, R. A., Edwards, P. M., Parrish, D. D., Gilman, J. B., Kuster, W. C.,
1626 Mielke, L. H., Osthoff, H. D., Tsai, C., Pikel'naya, O., Stutz, J., Veres, P. R., Roberts, J. M.,
1627 Griffith, S., Dusanter, S., Stevens, P. S., Flynn, J., Grossberg, N., Lefer, B., Holloway, J. S.,
1628 Peischl, J., Ryerson, T. B., Atlas, E. L., Blake, D. R., and Brown, S. S.: Chlorine as a primary
1629 radical: evaluation of methods to understand its role in initiation of oxidative cycles,
1630 Atmospheric Chemistry and Physics, 14, 3427–3440, <https://doi.org/10.5194/acp-14-3427-2014>,
1631 2014.
- 1632 Zhang, D. and Iwasaka, Y.: Chlorine deposition on dust particles in marine atmosphere,
1633 Geophysical Research Letters, 28, 3613–3616, <https://doi.org/10.1029/2001GL013333>, 2001.
- 1634 Zhang, Q., Alfarra, M. R., Worsnop, D. R., Allan, J. D., Coe, H., Canagaratna, M. R., and
1635 Jimenez, J. L.: Deconvolution and Quantification of Hydrocarbon-like and Oxygenated Organic
1636 Aerosols Based on Aerosol Mass Spectrometry, Environ. Sci. Technol., 39, 4938–4952,
1637 <https://doi.org/10.1021/es048568l>, 2005.
- 1638 Zhao, Y. and Gao, Y.: Acidic species and chloride depletion in coarse aerosol particles in the US
1639 east coast, Science of The Total Environment, 407, 541–547,
1640 <https://doi.org/10.1016/j.scitotenv.2008.09.002>, 2008.
- 1641 Ziemba, L. D., Griffin, R. J., Whitlow, S., and Talbot, R. W.: Characterization of water-soluble
1642 organic aerosol in coastal New England: Implications of variations in size distribution,
1643 Atmospheric Environment, 45, 7319–7329, <https://doi.org/10.1016/j.atmosenv.2011.08.022>,
1644 2011.
- 1645 Zorn, S. R., Drewnick, F., Schott, M., Hoffmann, T., and Borrmann, S.: Characterization of the
1646 South Atlantic marine boundary layer aerosol using an aerodyne aerosol mass spectrometer,
1647 Atmospheric Chemistry and Physics, 8, 4711–4728, <https://doi.org/10.5194/acp-8-4711-2008>,
1648 2008.
- 1649 Zuidema, P., Alvarez, C., Kramer, S. J., Custals, L., Izaguirre, M., Sealy, P., Prospero, J. M., and
1650 Blades, E.: Is Summer African Dust Arriving Earlier to Barbados? The Updated Long-Term In
1651 Situ Dust Mass Concentration Time Series from Ragged Point, Barbados, and Miami, Florida,
1652 Bulletin of the American Meteorological Society, 100, 1981–1986,
1653 <https://doi.org/10.1175/BAMS-D-18-0083.1>, 2019.

1654